

NASA TECHNICAL NOTE



NASA TN D-4827

21

NASA TN D-4827

LOAN COPY: RETURN TO
AFWL (WLIL-2)
KIRTLAND AFB, N

0131642



TECH LIBRARY KAFB, NM

COMPARISON OF SMALL
WATER-GRAPHITE NUCLEAR ROCKET
STAGES WITH CHEMICAL UPPER STAGES
FOR UNMANNED MISSIONS

by M. Ray Clark, Gary D. Sagerman, and Gerald P. Lahti

*Lewis Research Center
Cleveland, Ohio*



COMPARISON OF SMALL WATER-GRAPHITE NUCLEAR ROCKET STAGES
WITH CHEMICAL UPPER STAGES FOR UNMANNED MISSIONS

By M. Ray Clark, Gary D. Sagerman, and Gerald P. Lahti

Lewis Research Center
Cleveland, Ohio

NATIONAL AERONAUTICS AND SPACE ADMINISTRATION

For sale by the Clearinghouse for Federal Scientific and Technical Information
Springfield, Virginia 22151 - CFSTI price \$3.00

ABSTRACT

Payload performance and the radiation environment characteristics of this small reactor type (200 to 600 MW power) in a nuclear upper stage are considered. Payload dose criteria indicate that any shielding requirement would be based on propellant heating considerations. Several approaches to propellant heating, including subcooled or slush hydrogen propellant and shielding, are compared. Potential performance gains are outlined for the Saturn IB and 260-inch solid launch vehicles when employing orbital nuclear start, a single engine firing, optimum nuclear thrust, and subcooled hydrogen propellant. Payload sensitivity to the nuclear-stage jettison weight and to the shielding approach to propellant heating is illustrated.

CONTENTS

	Page
SUMMARY	1
INTRODUCTION	2
SMALL-NUCLEAR-STAGE WEIGHT ESTIMATE	3
Water-Graphite Reactor Description and Weight	3
Engine Component Weight	4
Upper-Stage Hardware Weight	6
WEIGHT PENALTY DUE TO RADIATION ENVIRONMENT	9
Payload Requirements for Radiation Protection	9
Nuclear Heating of Propellant	11
DESCRIPTION OF LAUNCH VEHICLES AND CHEMICAL UPPER STAGES	14
PAYLOAD PERFORMANCE COMPARISON	15
Trajectory Ground Rules	15
Orbital Start Requirement for Nuclear Rocket Engine	16
Selection of Optimum Nuclear-Stage Thrust	17
Comparison of Nuclear and Chemical Upper-Stage Performance	20
Nuclear-Stage Propellant Requirements	24
Sensitivity to Nuclear-Stage Hardware Weight Estimate	25
Sensitivity to Approach to Nuclear Propellant Heating	26
CONCLUDING REMARKS	27
APPENDIXES	
A - DETAILS OF ENGINE COMPONENT WEIGHT ESTIMATE	31
B - PAYLOAD RADIATION LEVELS FOR UNMANNED MISSIONS	34
C - DETAILS OF RADIATION DOSE AND PROPELLANT HEATING CALCULATIONS	37
D - NUCLEAR HEATING OF PROPELLANT	41
REFERENCES	52

COMPARISON OF SMALL WATER-GRAPHITE NUCLEAR ROCKET STAGES WITH CHEMICAL UPPER STAGES FOR UNMANNED MISSIONS

by M. Ray Clark, Gary D. Sagerman, and Gerald P. Lahti

Lewis Research Center

SUMMARY

A study of the small, low-thrust, water-graphite nuclear rocket (200 to 600 MW power and Phoebus-NERVA reactor power density) was prompted by potential application as upper-stage propulsion for unmanned missions. The choice of reactor type stemmed from (1) past studies at Lewis of a range of tungsten water-moderated nuclear reactor sizes and (2) potential development-time reduction by employing the extensive Phoebus-NERVA graphite-fuel-element experience. In this study, the main aspects considered in the use of a small nuclear upper stage in place of a chemical stage were (1) the relation of radiation environment to payload and propellant heating and (2) the effect of the nuclear rocket's higher specific impulse and engine weight on relative payload performance.

The payload dose criteria of 10^6 rads of gamma rays and 10^{13} neutrons per square centimeter of fast neutrons indicates that any shielding requirement would be based on propellant heating considerations. Of the several approaches to propellant heating compared, use of subcooled or slush hydrogen propellant offered the least penalty and typically required cooling to the range of hydrogen triple point (14 K) and 20 percent solid hydrogen-liquid mixtures. The shielding approach, which is representative of the maximum penalty, required as much as 600 kilograms of shadow shield, which represents about a 40-percent increase in engine weight.

A comparison was made between chemical and nuclear upper-stage performance when employing orbital nuclear start, optimum nuclear thrust, and subcooled hydrogen propellant. Consideration of launch vehicles compatible with the unmanned mission payload range showed (1) no payload gain using the Atlas-Centaur and (2) potential gains using the larger Saturn IB and 260-inch solid - S-IVB launch vehicles with optimum reactor powers of 300 to 600 megawatts for typical Jupiter, Saturn, and solar probe missions. Substituting the shielding approach to propellant heating neutralized some areas of the potential nuclear-stage performance gain.

INTRODUCTION

An extensive research and development effort in nuclear rocket technology is currently centered about the use of a graphite fuel-element material. The nuclear reactors currently envisioned for this fuel-element type are of relatively high power and large size compared with the small nuclear reactors considered herein. As one example, the NERVA II nuclear rocket reactor (ref. 1) is a recent high-power design with a power of about 5000 megawatts and a thrust of 1.11×10^6 newtons (250 000 lb). NERVA I has a thrust of 333 000 newtons (75 000 lb) and a reactor power of 1500 megawatts. In contrast, in this study reactor powers from about 200 to 600 megawatts are of concern.

This small-water-graphite-reactor performance study is an outgrowth of nuclear rocket studies at Lewis, which were concurrent with the graphite development effort. At Lewis the feasibility of a 1500-megawatt, tungsten, water-moderated nuclear rocket engine (ref. 2) was investigated. Some study was also devoted to smaller tungsten reactors in the 200-megawatt range, and the effort then evolved into this study. The impetus for the change to graphite was the desire to take advantage of the extensive graphite-fuel-element development to shorten potential development time. The 200-megawatt power range was chosen in order to investigate nuclear rocket performance at much lower reactor sizes and powers in the vicinity of the minimum critical nuclear size.

The water-graphite reactor study was reported in reference 3; this study, which is supplementary to that reference, was conducted to investigate the small-reactor performance when considered in the total nuclear upper stage and compared with chemical upper-stage counterparts. These smaller nuclear stages are potentially applicable to the range of unmanned missions. The unmanned mission payload range is roughly 115 to 13 600 kilograms (250 to 30 000 lb), and the comparison of nuclear and chemical upper stages was therefore made using a range of launch vehicles compatible with this payload range. The launch vehicles considered are the Atlas, the Saturn IB, and the 260-inch solid - S-IVB.

Several (unpublished) related studies have been performed by Los Alamos Scientific Laboratory, Aerojet-General, Westinghouse Astronuclear Laboratory, and Battelle Memorial Institute concerning, respectively, a small zirconium hydride - graphite nuclear reactor, an overall small-nuclear-rocket engine design, a small version of the NERVA type of nuclear reactor, and a performance and cost analysis of a generalized nuclear upper stage with detailed consideration of mission applications. Engine component weight estimates from the Aerojet-General data are also applicable to the small water-graphite reactor and were employed in this study. Detailed mission applications and relative development and production costs compared with alternate means of propulsion were not considered.

In comparing nuclear and chemical upper stages, the main aspects evaluated were (1) the performance penalty due to the added effect of radiation environment on both the unmanned payload and the propellant heating and (2) the performance effect of the nuclear rocket's higher specific impulse and engine weight. Both these aspects were evaluated in terms of the resultant payload performance of the nuclear stage relative to that of chemical upper stages.

The investigation proceeded in basically the following order:

(1) An engine component weight estimate was added to reactor weights based on the water-graphite reactor design defined in reference 3 to obtain total engine weight variation with reactor power.

(2) An estimate of a variable nuclear-stage hardware weight (total stage jettison weight minus engine weight and any shielding or other weight penalty for the radiation field) as a function of propellant loading was added so that the nuclear-stage size and propellant loading could be varied over a range of mission energies.

(3) Consideration was then given to any additional weight penalty due to the radiation field, with the payload effects and propellant heating effects treated separately. Several approaches for treating the propellant heating interaction were compared.

(4) The three stage weight components were then combined to define the variable nuclear-stage size for the payload performance analysis.

(5) The variation of the fairly substantial nuclear engine weight with reactor power and, hence, thrust was used to optimize nuclear-stage payload performance for each launch vehicle.

(6) Several fixed chemical upper-stage designs were defined, and a comparative analysis of payload performance against mission energy for nuclear and chemical upper stages was made for several typical launch vehicles. Several typical types of unmanned mission are indicated on the performance curves over the mission energy range, and the approximate areas of potential usefulness of a nuclear upper stage with a small water-graphite nuclear rocket are indicated in terms of launch vehicle class and mission energy.

(7) Selected performance comparisons were modified to show the effect on each comparison resulting from heavier weight penalty approaches to the treatment of the radiation field interaction.

SMALL-NUCLEAR-STAGE WEIGHT ESTIMATE

Water-Graphite Reactor Description and Weight

The water-graphite reactor core consists of clusters of graphite fuel elements supported by tie-tubes of a high-temperature nickel-chromium alloy. Water flow in the tie-tubes acts as a coolant and also enhances the neutron thermalization properties of the

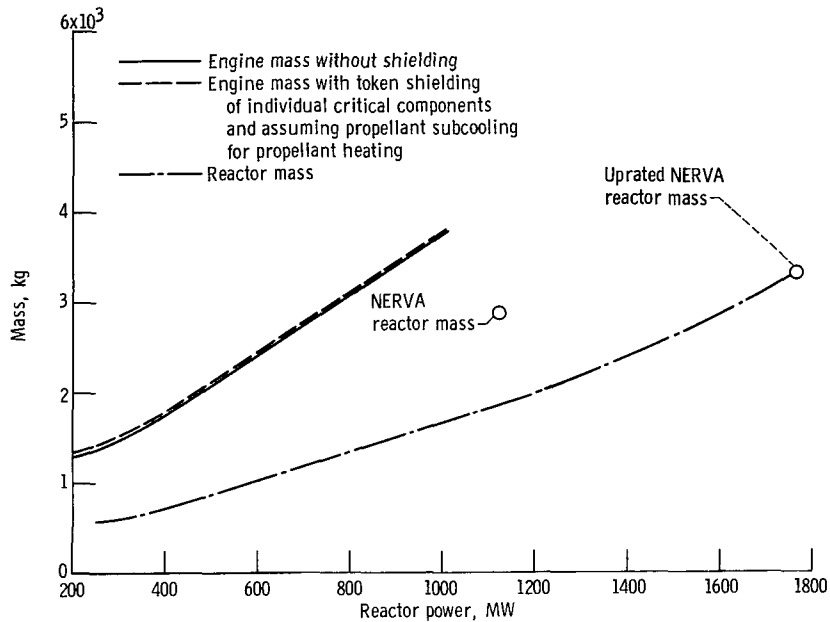


Figure 1. - Small water-graphite nuclear rocket mass.

graphite, thereby resulting in smaller possible core sizes. The radial reflector is 90 volume percent beryllium with a 10 volume percent water coolant flow, and the inlet and axial reflector is composed of a beryllium support plate and the water flow plenums. The radial reflector thickness is varied over most of the range of reactor power to achieve criticality for these small, reactivity-limited cores. The reactor power for each core size is determined by the maximum allowable, thermal-stress-limited, power density of NERVA II technology. Further details of the reactor description are given in reference 3. The curve of reactor weight against reactor power used in this study was obtained from the analysis in reference 3 and is shown in figure 1. The high-power range of the estimate is based on an extrapolation using reference 4 for NERVA reactor weight at 1120 megawatts, but uprated to 1760 megawatts to represent the power density of NERVA II technology, as shown in figure 1.

Engine Component Weight

In addition to reactor weight, several other major engine weight components must be reasonably estimated over the range of reactor power and thrust being considered. These weight components are a large percentage of the total engine weight; and, when coupled with stage hardware weight components of equal importance, they can have a strong effect on the validity of the calculated payload of small nuclear rocket stages.

Estimates, as such, cannot be extremely accurate compared with detailed design

studies for every reactor size and power. Nevertheless, by including a fairly consistent and detailed list of component categories for engine and stage component weights and tying them to a few previously studied design points, a clearer and more accurate representation than that obtained from one lumped parameter was made.

Estimates were made for the pressure vessel, nozzle, propellant turbopump, water turbopump, flow-line assemblies, tank valve assemblies, upper and lower thrust structure, diagnostic instrumentation system, engine control system, and pneumatic system. Two additional weight components, sometimes considered to be engine components, were assumed to be included in stage hardware weight components instead. These are the roll control system and the thrust vector (excluding gimbal) control system.

Such component terminology is essentially consistent with the definitions for the NERVA 1120-megawatt engine as given in references 4 and 5. These categories are also consistent with the TRW Space Technology Laboratories (STL) study (refs. 6 and 7), which optimized the nuclear-module-concept engine and stage (propellant capacity of about 159 000 kg (350 000 lb) and reactor power of about 5000 MW) for the manned, nu-

TABLE I. - ENGINE COMPONENT WEIGHT ESTIMATE

Component	Reactor power, MW					NERVA, 1120 MW
	200	300	400	600	1000	
	Weight, kg					
Reactor	568	600	705	1018	1664	3313
Pressure vessel	50	52	60	106	318	425
Nozzle	123	154	186	253	386	349
Propellant turbopump	75	80	92	109	142	152
Water turbopump	19	20	23	27	35	----
Flow-line and tank valve assemblies	158	191	225	296	^a 273	308
Upper and lower thrust structure and thrust vector structure	75	109	146	221	371	418
Diagnostic instru- mentation system	68	68	70	73	77	80
Engine control system	126	146	166	206	287	314
Pneumatic system	27	45	65	105	185	210
Engine weight without shield	1289	1465	1738	2414	3738	5567

^aReverted to single hydrogen flow system with no water loop.

clear propulsion missions of the 1975 to 1990 time period.

Engine component weight estimates for the small nuclear stage at the high-power end of the 200 to 1000 megawatt power range were taken from the STL study, which in turn is based on the Aerojet-General Corporation NERVA engine weight data at 1120 megawatts (ref. 4). For the low-power end of the range, Aerojet-General Corporation, the NERVA engine contractor, was considered to be the source of the best available component design data, and engine component weights generated in the 200-megawatt power range for an Aerojet study of a small nuclear rocket engine were also employed in this study.

A description of the treatment of each engine component weight for the reactor power range of 200 to 1000 megawatts is given in appendix A. Table I itemizes these weight estimates for several sizes of the small water-graphite nuclear rocket using the NERVA definition of engine components with additional components as required for the water-moderator - coolant loop. Figure 1 summarizes the total engine weight estimate against reactor power used for this study. For small water-graphite reactor weights of 570 to 1020 kilograms over the range of 200 to 600 megawatts, the engine weight without shielding is 1290 to 2420 kilograms.

Upper-Stage Hardware Weight

One of the more difficult problems associated with this study was that of estimating jettison weights for the nuclear stages considered. The jettison weight is made up of the engine weight plus the remaining structure and system weights (including residuals) which is referred to as hardware weight. The weight of the engine is constant for a given engine thrust or power, and the values used are shown in table II.

Hardware weights for a wide range of propellant loadings were required, although

TABLE II. - WEIGHT OF NUCLEAR ENGINE

Nuclear reactor power, MW	Nuclear engine thrust, N	Engine weight, kg
200	44 480	1334
300	66 720	1510
400	88 960	1783
600	133 440	2459
1000	222 400	3783

TABLE III. - RIFT OPERATIONAL VEHICLE WEIGHT TABULATION

[Weight in kg.]

Structure:	
Fuel container	9 760
Forward skirt	944
Aft skirt	992
Paint and sealer	31
Total	11 727
Propulsion system (nuclear engine and accessories removed):	
Purge system	108
Fuel system	530
Stage control system	211
Total	849
Equipment and instrumentation:	
Structure for equipment and instrumentation	272
Guidance system	7
Control-system electronics	9
Telemetry and measuring equipment (adjusted)	74
Propellant utilization	3
Electrical system	744
Range safety equipment	64
Total	1 173
Residual and reserve propellant:	
Propellant, pressurized gas	252
Propellant, trapped	364
Service items	91
Total	707
Standard propellant	76 000
Design reserve	427
Instrument unit	1 023

design of nuclear stages was beyond the scope of this study. Table III presents a weight tabulation for a proposed operational configuration of a nuclear stage which was designed for the RIFT program. The stage, which is fully described in reference 8, is the result of extensive analysis and design. As such, it was considered to be a sound basis for hardware weight estimates at its given propellant loading of 75 854 kilograms (167 230 lb) of liquid hydrogen. A hardware weight to propellant weight ratio W_{hw}/W_p of 0.209, excluding the engine and shielding, was calculated for the RIFT operational vehicle.

In order to cover the entire range of propellant weights required for this study, it was necessary to estimate W_{hw}/W_p at low propellant weights. Beginning with the Centaur hydrogen-oxygen stage described in reference 9, all oxidizer related weights, engines, engine controls, and other equipment not required for nuclear-stage operation,

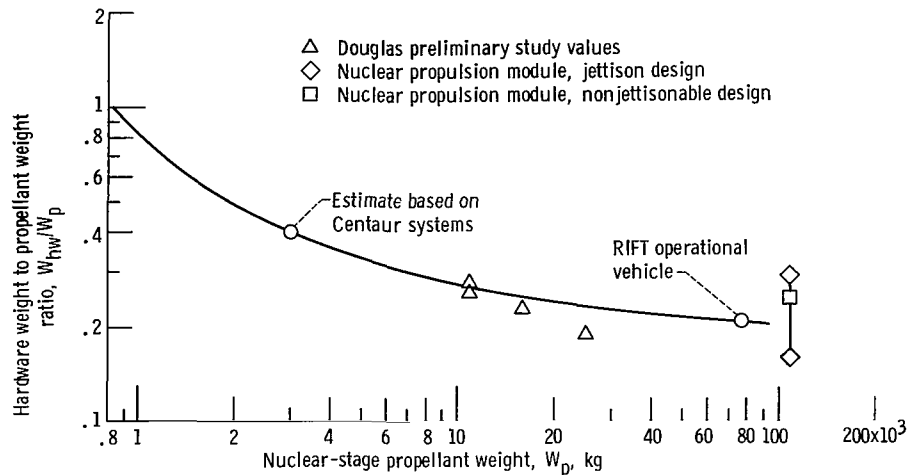


Figure 2. - Nuclear-stage hardware weight estimation. (Stage hardware weight includes all nuclear-stage jettison weight except engine weights which are shown in table II.)

were removed. Permanent insulation was added, and hydrogen residuals were adjusted. A hardware weight to propellant weight ratio of 0.401 resulted. Based on the two available points and previous experience with chemical stages, the curve shown in figure 2 was constructed. All nuclear-stage hardware weights in this report are based on figure 2.

For comparison purposes, estimated values of W_{hw}/W_p at 10 886, 15 876, and 24 947 kilograms (24 000, 35 000, and 55 000 lb) of propellant are also shown in figure 2. These values were obtained from an unpublished Douglas preliminary study of nuclear stages using modified S-IVB stage design; they tend to support the assumed curve.

More recent data for a larger nuclear stage than the RIFT vehicle became available after this analysis was performed and are also shown in figure 2 for comparison. These data points are the result of design studies for the nuclear propulsion module (refs. 10 and 11) at 104 300 kilograms (230 000 lb) of propellant. The final stage design from these studies (ref. 10) employs a jettisonable outer shell to carry ascent loads. Therefore, the two end points for the module design with and without the jettisonable shell are given to approximately represent the range of W_{hw}/W_p for this type of design. The jettisonable meteoroid insulation shield for the extended space exposure of interplanetary engine starts was subtracted in arriving at these values to compare more closely with orbital stage operation in this report. An interim design (ref. 11) in the evolutionary process of those recent studies is also shown in figure 2 and represents a nonjettisonable load-carrying shell design more comparable to the RIFT, S-IVB, and Centaur vehicles. The higher value of W_{hw}/W_p than for the RIFT vehicle is expected because of the longer space exposure times for the interplanetary missions discussed in reference 11. This weight penalty was not readily adjustable in this case to arrive at a better comparison.

WEIGHT PENALTY DUE TO RADIATION ENVIRONMENT

Use of a nuclear upper stage introduces a neutron and gamma radiation environment, not otherwise encountered in space. Therefore, in order to compare chemical and nuclear upper stages, the radiation field interaction with the unmanned payload and the propellant heating must be considered. An estimate of any nuclear-stage weight penalty and, hence, payload penalty can then be defined for the radiation environment effects.

It should be noted that in considering the stage radiation environment, several specific reactor sizes of odd powers were employed in treating the reactor power variable. Later, in the nuclear-stage performance analysis it was feasible to employ even power levels of hundreds of megawatts. The specific sizes, corresponding to powers of 432, 254, and 181 megawatts, were defined in the previous water-graphite reactor study (ref. 3) and are required to treat specifically defined geometries in the radiation calculations. The computer program QADHD (ref. 12), written to evaluate both the propellant heating and the time-integrated dose from radiation in nuclear rocket geometries, was used for the calculations.

Payload Requirements for Radiation Protection

In treating the payload - radiation environment interaction for the unmanned missions, the radiation damage to electronic equipment was assumed to be the limiting factor. Therefore, the approach was to set and meet cumulative radiation dose limits for radiation damage. Stage equipment susceptible to radiation damage could be positioned in the forward skirt area above the propellant tank and, hence, may be considered under the same criterion as payload equipment. Engine components (such as turbopump, actuators, etc.) in the vicinity of the reactor were assumed to be radiation hardened as required or locally shielded by small amounts of shielding.

Reference 13 indicates that electronic equipment can be designed so that cumulative doses of 10^6 rads of gamma rays and 10^{13} neutrons per square centimeter of fast neutrons will not degrade their performance. Doses of this level therefore formed the basis for the allowable time-integrated radiation dose to electronic equipment. A payload position is conservatively established as the surface level of the initial propellant mass before engine firing. The propellant serves as a shield between the engine and the payload but is continuously reduced during engine operation by consumption of the propellant. A cylindrical tank 6 meters in diameter with a truncated conical bottom section was considered in the dose calculations. Further details of the calculations and geometry are given in appendixes B and C.

The cumulative fast-neutron and gamma-ray doses for variable initial propellant load and the corresponding separation distance between the reactor and payload are shown

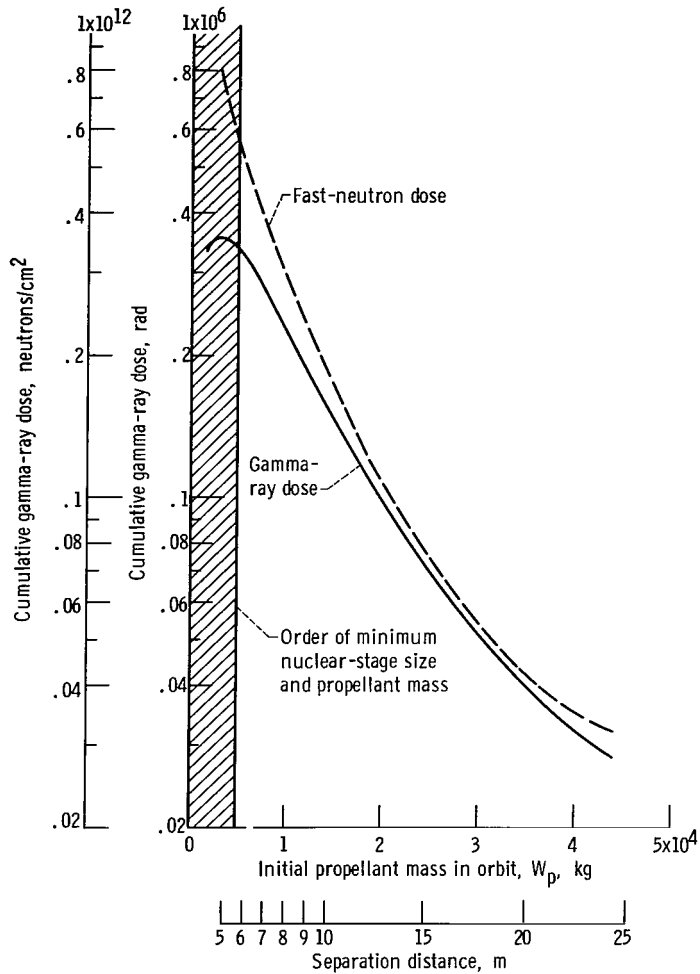


Figure 3. - Cumulative gamma-ray and fast-neutron dose at payload.

in figure 3. These values are independent of reactor power level and corresponding propellant flow rate since the exposure time, or time to empty the tank, is inversely proportional to the power. No shielding other than the gradually decreasing propellant mass and some reactor structure is involved.

Neither the fast-neutron dose nor gamma-ray dose are greater than the allowable radiation dose criteria. The fast-neutron dose climbs rapidly at low propellant loadings and separation distances. However, a minimum useful nuclear-stage propellant loading is of the order of about 5000 kilograms of liquid hydrogen from nuclear-stage performance and mission considerations. This minimum loading limits the fast-neutron dose attained at low propellant loads to an order of magnitude below the criterion. Therefore, according to the criteria used in this study, no radiation shielding is required in unmanned missions for the potential payload radiation damage effects.

Nuclear Heating of Propellant

The radiation field can affect the nuclear-stage performance by adding a weight penalty for an additional propellant heating component besides the usual aerodynamic and space environment heating. This propellant heating aspect of the nuclear stage was evaluated in terms of several possible design alternatives for coping with nuclear heating. These approaches are (1) direct propellant boiloff from initially nearly saturated liquid conditions, (2) propellant supply at subcooled conditions for heating during engine operation to saturation conditions, (3) higher pressure tank design to maintain saturated liquid in the last moments of engine run time, and (4) nuclear shielding to reduce gamma and neutron heating to a negligibly low level. The range of weight penalties for these various approaches is approximately determined to show their relation.

One foundation on which this comparison of approaches rests is the choice of the required value of the net positive suction pressure (NPSP) (i. e., tank pressure minus vapor pressure corresponding to the propellant temperature value) at the tank bottom. The required value of NPSP imposes the pump cavitation limit on propellant heating. Reference 14 indicates that the current status of pump technology may allow the use of a zero NPSP condition at the tank bottom as the tank approaches liquid exhaustion. The pump design eliminates or minimizes main pump cavitation in this condition by means of a low-speed inducer ahead of the pump. Use of the zero NPSP condition minimizes the tank design pressure required from pump considerations. It also eliminates the unusable propellant occurring in the case of a positive NPSP - full flow rate requirement coupled with a tank pressure equivalent to vapor pressure at liquid exhaustion. The zero NPSP requirement is used in this comparison of design approaches to define the relation between tank design pressure and final propellant temperature.

For the purposes of this comparison, several simplifying assumptions and approximations were made concerning the propellant heating and thermodynamic and flow processes within the tank. First, the nuclear tank wall heating and its propellant heating contribution were neglected. Nuclear wall heating is only about 12 percent as large as the nuclear bulk heating for a typical tank wall of 0.038-centimeter- (0.015-in. -) thick stainless steel. Therefore, because of geometrical considerations and partial radiation of the nuclear wall heating to space, the total nuclear heating is adequately represented by calculations of the bulk heating. Only the space environment wall heating was estimated, to illustrate the degree of this nonnuclear heating component during engine operation.

Second, the turbulent bulk mixing produced by the nuclear bulk heating of the propellant (refs. 15 and 16) was assumed to disrupt any concurrent sidewall heating boundary layer from the space environment wall heating. This effect is noted in references 15 to 17, although to a lesser extent, which lends some support to the assumption. The

stratified thermal layer below the propellant surface, which results from the sidewall boundary layer flow, was therefore neglected. A complete bulk mixing flow model was therefore used to obtain propellant temperature rise from both nuclear bulk heating and a space environment wall heating component.

If some degree of stratification does actually remain in the presence of nuclear bulk heating, this flow pattern would result in the layers near the surface attaining saturation temperature earlier in the total run time as they enter the bottom region of turbulent mixing. Subsequent heating near the tank bottom could result in vapor formation, added boiloff, and some vapor ingestion into the pump in the real situation. Some amount of vapor ingestion into the pump at zero NPSP is acceptable, as noted in reference 14, and it provides some leeway for estimates based on complete bulk mixing. This whole aspect requires further detailed study of the thermodynamic and flow processes during propellant heating, but it is beyond the scope of this study.

Third, the initial or nonnuclear heating phase was neglected. This phase consists of heating during ground hold, during ascent through the atmosphere, and during orbital stay-time before nuclear-stage operation. This heating phase is essentially the same no matter what design approach is used for the nuclear propellant heating. Even nominal propellant subcooling at typical propellant temperature and pressure conditions is assumed to be sufficient to absorb this heating. In the later-stage performance calculations this boiloff prior to nuclear engine start was also not considered. Further study may be required in a more detailed analysis to show its negligible extent.

The relative weight penalties of the four approaches are defined as the increase of the initial nuclear-stage weight in each case relative to initial stage weight with no propellant heating and with propellant at a typical supply temperature of 20.4 K and typical tank design pressure of 17.2 newtons per square centimeter (25 psia). Any additional shielding, additional propellant for boiloff, and/or additional tank plus insulation weight to encompass the total propellant required in each case are the primary-stage weight increases induced by the propellant heating. All other stage weight components were considered to be constant.

The relative penalties of the four approaches are summarized as follows:

- (1) Direct propellant boiloff
 - (a) Propellant mass boiloff during nuclear engine operation
 - (b) Tank mass increase to enclose additional boiloff mass
- (2) Propellant subcooling, no penalty
- (3) Tank pressurization, tank mass increase due to design pressure increase
- (4) Reactor shielding, shield mass addition

The analysis of each of these approaches is presented in appendix D. In the case of propellant subcooling, the extent of the required subcooling is estimated in lieu of a penalty.

In figure 4, these relative penalties are plotted against the useable propellant weight

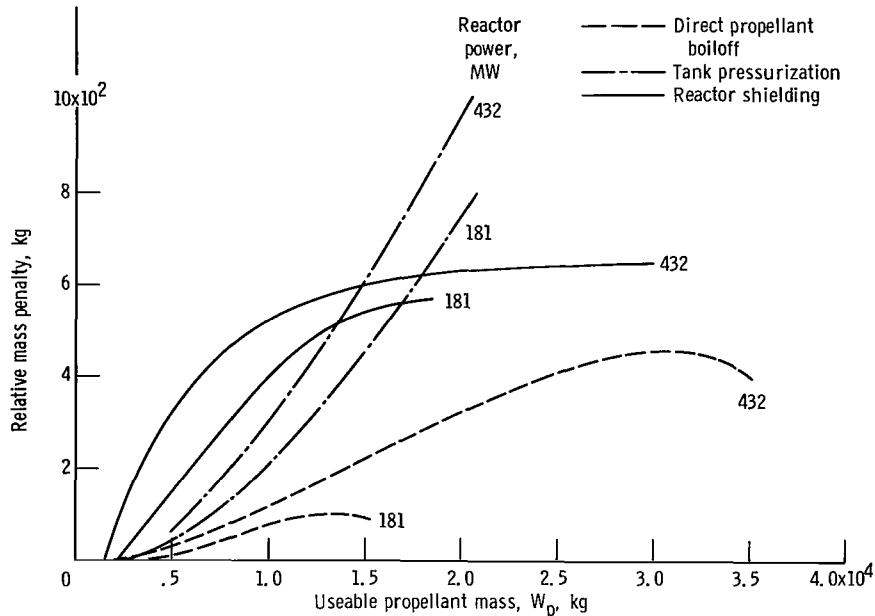


Figure 4. - Comparison of approaches to propellant heating. (Nonnuclear heating phase boiloff neglected as constant in all approaches; abscissa represents zero penalty of propellant subcooling.)

W_p . A constant value of W_p is indicative of approximately constant nuclear-stage performance, especially if the reactor power, and hence thrust, is held constant. The range of penalty in figure 4 for varying reactor power is bracketed for each approach to propellant heating by showing an upper curve for 432 megawatts reactor power and a lower curve for 181 megawatts reactor power.

Lower reactor power, for the same W_p and, therefore, total reactor energy release, shows a slight advantage in figure 4. This advantage is due to smaller core diameter and greater radial reflector thickness at about the same overall reactor diameter for these criticality limited reactors. Increased radial reflector thickness has some shielding value in the two-dimensional propellant heating situation.

The boiloff penalty shown in figure 4 was calculated by assuming venting at a constant rate after the depletion of the nominal propellant subcooling. The magnitude of the boiloff penalty is dependent on the initial weight delivered to orbit by the launch vehicle. The two curves in figure 4 for 432 and 181 megawatts were selected to approximate this launch vehicle dependence. The upper curve for 432 megawatts corresponds to the 260-inch solid - S-IVB - nuclear-stage configuration for a 185-kilometer (100-n-mi) nuclear-stage launch orbit. These configurations are discussed in greater detail in the PAYLOAD PERFORMANCE COMPARISON section.

The propellant subcooling approach is, of course, the minimum weight approach at all propellant loadings. The analysis in appendix D shows that at about 20 000 kilograms

of propellant, subcooling in the range of the hydrogen triple point (14 K) is needed. At about 30 000 kilograms, a slush hydrogen mixture of about 20 percent solid hydrogen is needed. An operational system of this type is not a foregone conclusion at this time, but current studies have uncovered no insurmountable problems (refs. 18 to 21).

For the other approaches, the comparison shows a crossover point at about 15 000 kilograms of propellant, beyond which the shielding approach has a significantly lower penalty than tank pressurization. The direct boiloff approach shows the least penalty of the three.

For the purposes of the following payload performance comparison between nuclear and chemical upper stages in the remainder of the report, the propellant subcooling approach with no weight penalty was assumed for nuclear propellant heating. The nuclear-stage jettison weight estimate and performance calculations are appropriate to the propellant subcooling approach since no provision is made for major shielding or any other corresponding weight penalty. A token allowance of 45 kilograms (100 lb) was included in engine weight, however, for possible shielding of small individual critical components, as shown in figure 1. In the section Sensitivity to Approach to Nuclear Propellant Heating, the shield weight penalty is applied to several booster, nuclear upper-stage combinations to illustrate the effect of the maximum penalty approach on performance.

DESCRIPTION OF LAUNCH VEHICLES AND CHEMICAL UPPER STAGES

In order to compare the performance of the small nuclear upper stage with that of chemical upper stages, it was necessary to consider each of these stages on a variety of launch vehicles.

The Atlas-Centaur, Saturn IB, and 260-inch solid - S-IVB were selected as being representative of the range of launch vehicles on which the small nuclear upper stage might show desirable performance. In general, current launch vehicle data were used for all performance calculations. A description of the Atlas-Centaur configuration is available in reference 9. The Saturn IB and 260-inch solid - S-IVB are described fully in references 22 and 23, respectively, and were flown according to the ground rules consistent with those references.

The chemical upper stages considered are the presently available Centaur and Burner II and a conceptual hydrogen-fluorine upper stage (HFUS). The Centaur used in this study is consistent with that described in reference 9 with a few exceptions. The specific impulse used was 4350 newton-seconds per kilogram (444 lb force-sec/lb mass) instead of the reference value. The higher specific impulse is expected to be available in the time period for which the nuclear stage can be considered. Also, for the larger boosters (Saturn IB and 260-in. solid - S-IVB) where the Centaur was fully shrouded, 68 kilograms of permanent insulation was used in place of the jettisonable panels common

to the Atlas-based Centaur. When the hydrogen-fluorine stage was flown on top of Centaur, much of the Centaur guidance equipment was removed and sufficient guidance was placed in the HFUS to control both stages. This arrangement resulted in a reduction of about 180 kilograms in Centaur jettison weight. Other minor modifications were made in the Centaur to accommodate the Burner II and HFUS; however, they did not significantly affect the final performance, and, hence, they are not detailed here.

The Burner II is a small upper stage built around the TE-364 spherical solid propellant motor (Surveyor retrorotor). A nominal specific impulse of 2850 newton-seconds per kilogram (290 lb force-sec/lb mass) is delivered by the 653 kilograms of impulse propellants. The jettison weight of the Burner II configuration used in this report is 188 kilograms. A detailed description of the Burner II systems and performance characteristics is given in reference 24.

The hydrogen-fluorine upper stage (HFUS) is not a presently available stage, but is an estimate of the maximum performance possible consistent with current chemical propulsion design technology. A specific impulse of 4510 newton-seconds per kilogram (460 lb force-sec/lb mass) was assumed for the liquid-hydrogen - liquid-fluorine propellant combination. A propellant weight of 4080 kilograms and a thrust of 35 580 newtons were chosen based on a preliminary optimization study. A mass fraction (propellant weight/total stage weight) of 0.845 yielded a jettison weight of 742 kilograms.

PAYLOAD PERFORMANCE COMPARISON

Trajectory Ground Rules

All performance data in this report are the results of fully integrated flight trajectories obtained using a digital computer. A launch azimuth of 90° east of north is common to all calculations. A nuclear-stage specific impulse of 7850 newton-seconds per kilogram (800 lb force-sec/lb mass) was assumed and nuclear-stage jettison weights were obtained by using table II (p. 6) and figure 2 (p. 8). Chemical-stage performance characteristics and jettison weights were as indicated in the section DESCRIPTION OF LAUNCH VEHICLES AND CHEMICAL STAGES. Appropriate flight performance reserves were charged to each vehicle combination to account for dispersions from nominal values of performance parameters (such as thrust, specific impulse, etc.). Parking orbit ascent trajectories were used for all vehicle configurations, with the nuclear stage assumed to start from orbit with a single firing.

Performance data are presented as curves of payload against geocentric vis viva energy C_3 where

$$C_3 = v^2 - \frac{2\mu}{R}$$

and

V spacecraft velocity

μ gravitational constant of earth

R radius from center of earth to spacecraft

Geocentric vis viva energy is a measure of kinetic energy (specifically, twice the energy per unit mass) relative to the earth remaining after the spacecraft has escaped the earth. In this report C_3 is used instead of burnout velocity because, for a given mission, the required burnout velocity is a function of the orbital altitude, while the required C_3 is essentially independent of burnout altitude. Therefore, using C_3 as the mission parameter allows an equitable comparison of vehicles with different burnout altitudes.

Interstage weights consistent with previous studies performed at Lewis were used between all stages. However, the present study did not analyze any structural modification of the launch vehicles required to fly the various configurations described herein.

Orbital Start Requirement for Nuclear Rocket Engine

Suborbital startup of nuclear stages was not analyzed in this study. Suborbital start-up techniques are being studied in order to perfect a safe suborbital mode of operation for Saturn V third-stage application, as indicated by studies such as references 25 to 28. However, for the launch vehicles considered herein, only orbital start has been assumed. A 185-kilometer (100-n-mi) circular parking orbit was originally selected for performance calculations. The launch vehicle configuration involved delivered its maximum payload, which included the nuclear stage, to orbit. This nuclear-stage ignition weight was held fixed for the given launch vehicle. By selecting various energies, determining the amount of propellant required to accelerate the vehicle to each of the desired energies, and subtracting the jettison weight corresponding to the propellant used in each case, a curve of payload against vis viva energy was generated.

If due to a failure the nuclear stage should not leave the 185-kilometer orbit, or should succeed only in attaining an elliptical orbit with a low perigee, the lifetime of the orbit would be short (less than a day for the 185-kilometer circular orbit), and the re-entry of the nuclear stage could still present a radiation hazard. For this reason, it was decided to evaluate the performance penalty associated with starting the nuclear stage in higher orbit with a longer decay time. A 926-kilometer (500-n-mi) circular orbit with a lifetime of about 260 years was selected. Orbital lifetime decreases rapidly as the orbital altitude is lowered; for example, the orbital lifetime drops to about 1 year for a 460-kilometer (250-n-mi) circular orbit. So while the 926-kilometer orbit is conserva-

tive, it is not unreasonable. Data are presented for both orbital altitudes to show the upper and lower limits of performance which may be expected from the nuclear stage.

For departures from the higher orbit, the booster configuration burned out at perigee of an elliptical orbit with a perigee altitude of 185 kilometers and an apogee altitude of 926 kilometers. After coasting to apogee, a small earth-storable propulsion system with a specific impulse of 2990 newton-seconds per kilogram (305 lb force-sec/lb mass) and a mass fraction of 0.75 was used to place the nuclear stage and its payload in circular orbit at 926 kilometers. Again, by holding ignition weight fixed and allowing the nuclear-stage propellant weight and associated stage jettison weight to vary, a curve of payload against vis viva energy was generated.

Selection of Optimum Nuclear-Stage Thrust

It has been recognized herein that for the high-energy missions being considered, gravity losses would have a major effect on payload. The gravity losses may be decreased by increasing the reactor power or thrust of the nuclear stage. However, as the reactor power level is raised, the engine weight increases significantly, as seen in table II (p. 6). Hence, a trade-off must be made between engine weight and gravity losses to determine the reactor power level that will yield maximum payload. The results of an investigation to determine the best nuclear-stage power to use on each launch vehicle are shown in figures 5 to 8.

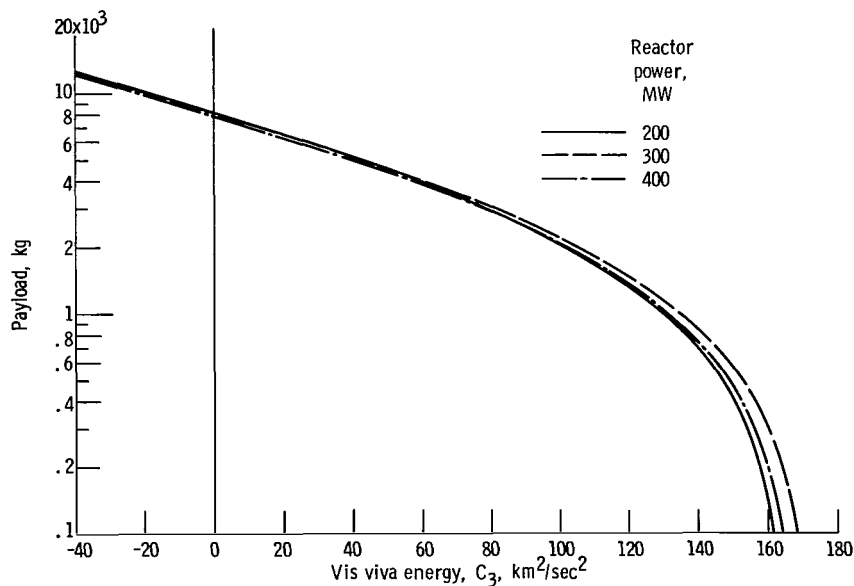


Figure 5. - Selection of nuclear-stage thrust for use on Saturn IB starting in 185-kilometer (100-n-mi) circular orbit.

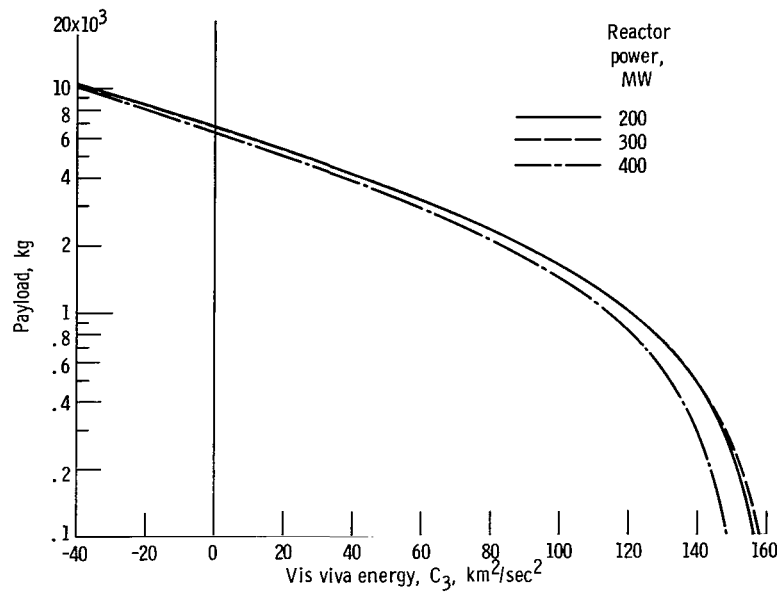


Figure 6. - Selection of nuclear-stage thrust for use on Saturn IB starting in 926-kilometer (500-n-mi) circular orbit.

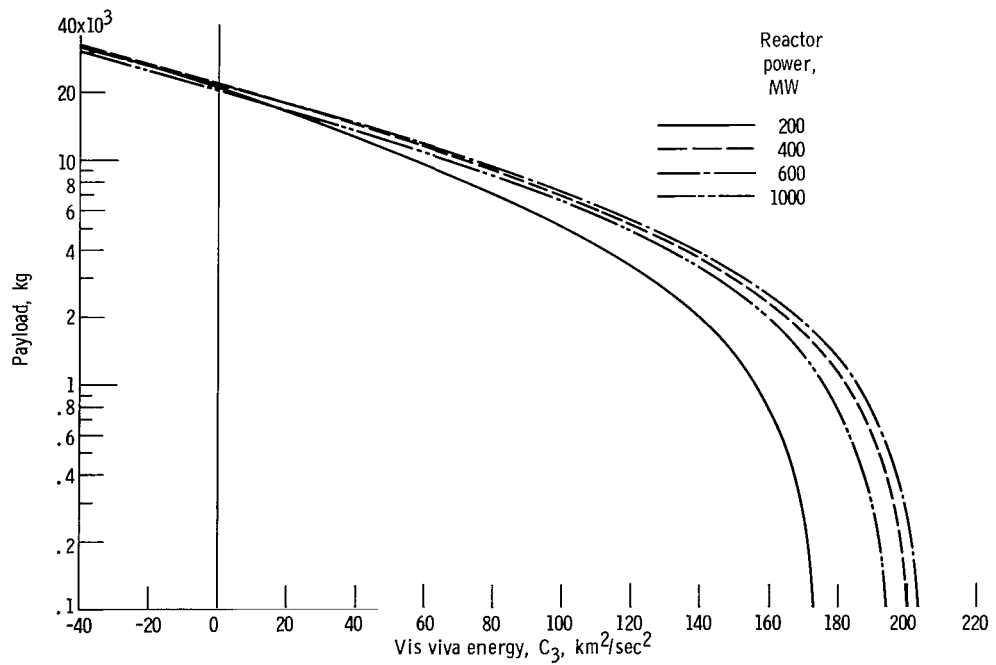


Figure 7. - Selection of nuclear-stage thrust for use on 260-inch solid - S-IVB starting in 185-kilometer (100-n-mi) circular orbit.

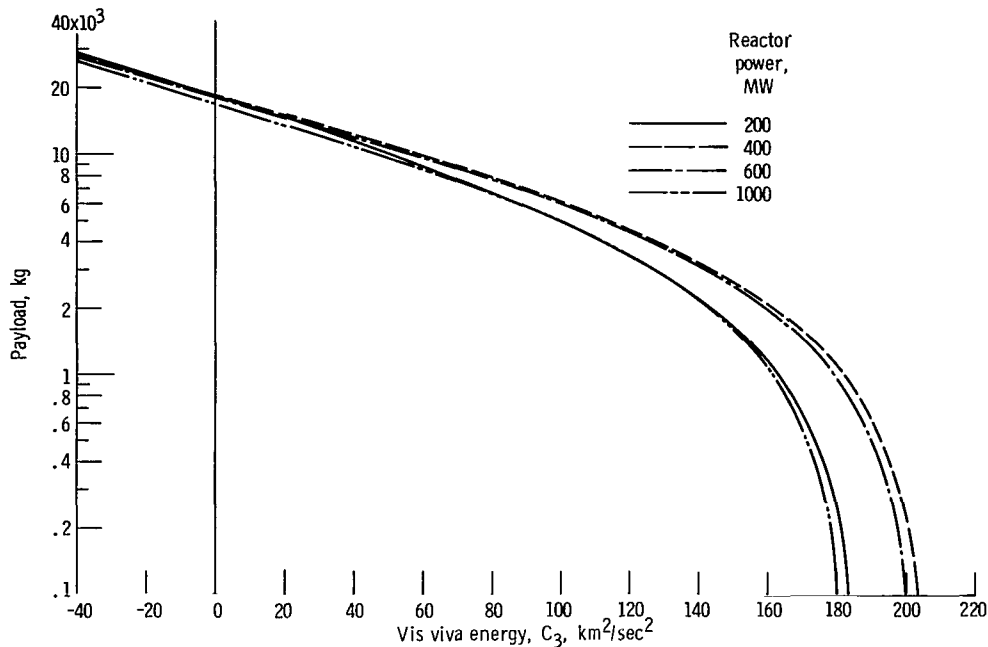


Figure 8. - Selection of nuclear-stage thrust for use on 260-inch solid - S-IVB starting in 926-kilometer (500-n-mi) circular orbit.

Figures 5 and 6 present payload against C_3 for nuclear stages of 200, 300, and 400 megawatts of reactor power on Saturn IB. These power levels correspond to thrusts of 44 480, 66 720, and 88 960 newtons (10 000, 15 000, and 20 000 lb) respectively, as shown in table II. Figure 5 is for nuclear-stage starts in the 185-kilometer circular orbits, and figure 6 is for 926-kilometer starts. The 300-megawatt stage was selected for use from 185 kilometers based on the performance advantage shown. The same 300-megawatt stage was picked for use from 926 kilometers although the 200-megawatt stage could be used with equal results.

Similar curves are shown in figures 7 and 8 for the 260-inch solid - S-IVB launch vehicle. Due to the larger initial weight available in orbit, reactor powers of 200, 400, 600, and 1000 megawatts were considered, which correspond to thrusts of 44 480, 88 960, 133 440, and 222 400 newtons (10 000, 20 000, 30 000, and 50 000 lb), respectively. For the nuclear-stage starts in the 185-kilometer orbit, shown in figure 7, the 600-megawatt stage was selected. The 400-megawatt stage was used for the 926-kilometer case on the basis of figure 8.

A reactor power of 200 megawatts was the minimum size allowed in this study due to a size limitation defined for the water-graphite reactors in reference 3. Hence, although the very low weights delivered to orbit by Atlas-Centaur indicate that lower thrusts would be optimum, the 200-megawatt engine was used for nuclear stages starting at both orbital altitudes on Atlas-Centaur.

The thrusts selected are used on the respective launch vehicles in the following performance comparisons.

Comparison of Nuclear and Chemical Upper-Stage Performance

Figures 9 to 14 show the payload capabilities of the various launch vehicle and upper-stage combinations studied. The energy levels of several missions of interest are indicated along the abscissa of each figure. It should be noted that, as previously mentioned, the nuclear-stage propellant capacity was allowed to vary to fit the energy requirement while the chemical stages were of specific sizes.

Figure 9 presents curves of payload against C_3 for chemical and nuclear stages on the Atlas-Centaur launch vehicle. Without the Centaur, the Atlas cannot place sufficient weight in orbit to make the use of a nuclear stage possible. Thus, the nuclear stage cannot be realistically compared with Centaur on this vehicle under the ground rules of this study. It is quickly evident from the figure that the nuclear stage is not competitive in a comparison with the HFUS or Burner II on the Atlas-Centaur; and, thus, use of nuclear propulsion on Atlas-Centaur was not considered further.

Curves showing the performance comparison between Centaur and the nuclear stage on the Saturn IB launch vehicle are presented in figure 10. The nuclear stage starting from 926 kilometers shows a small payload advantage above a C_3 of 30 kilometers

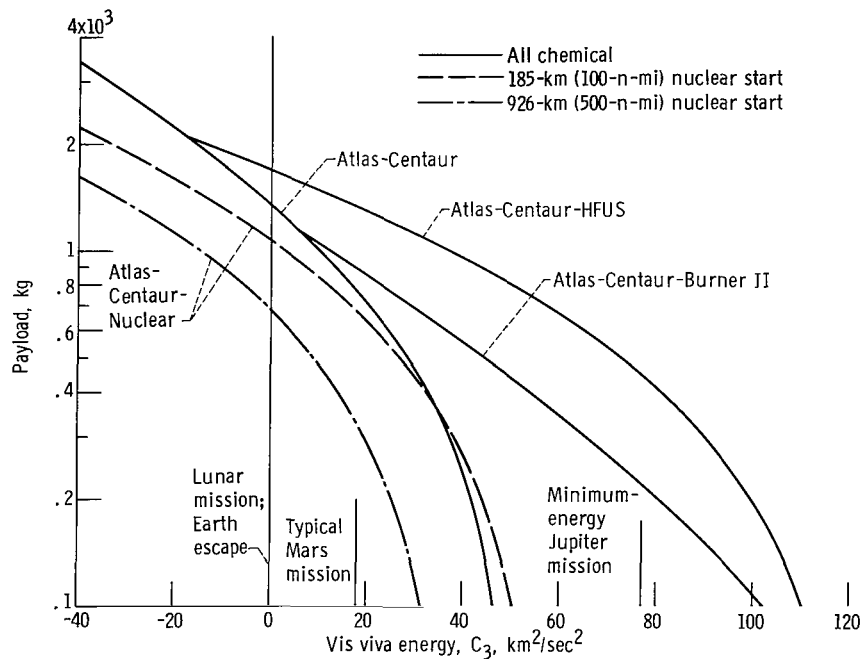


Figure 9. - Performance of nuclear and chemical upper stages on Atlas-Centaur. Reactor power, 200 megawatts.

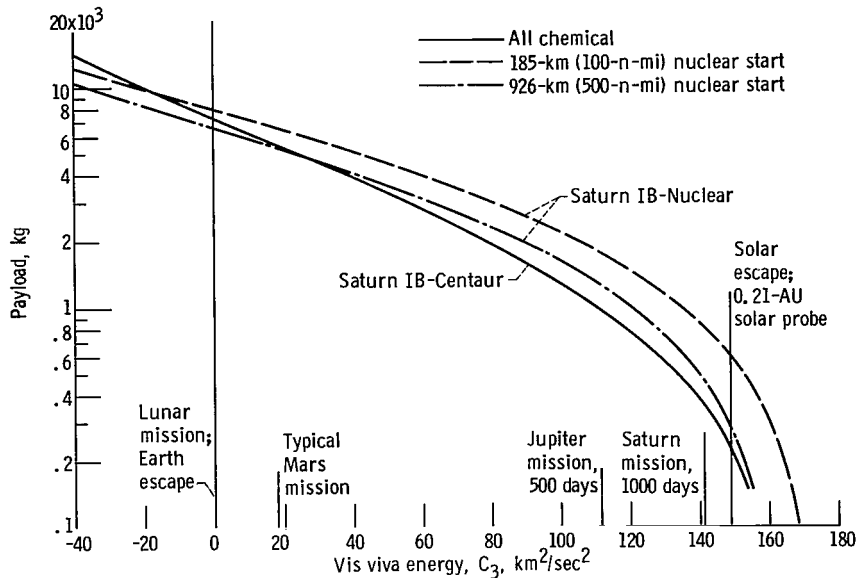


Figure 10. - Comparison of nuclear upper stages with Centaur on Saturn IB. Reactor power, 300 megawatts.

squared per second squared. However, if safety considerations allow the use of the 185-kilometer startup of the nuclear stage, a larger payload improvement is indicated. The Saturn IB - Nuclear (185) can deliver 605 kilograms to a solar escape or a 0.21-astronomical-unit solar probe which more than doubles the Saturn IB-Centaur payload for the same missions. The nuclear configuration also offers a payload improvement for the typical Jupiter and Saturn mission energies shown. Because of the low absolute magnitude of this improvement, however, the conclusion is subject to the accuracy of the nuclear stage and engine weight estimates.

Figures 11 and 12 show the effect of additional stages on both the nuclear and chemical Saturn IB-based vehicle combinations. It is evident from figure 11 that, while the Saturn IB - Nuclear(185) and the Saturn IB - Centaur - HFUS exhibit comparable performance at energies as great as 100 kilometers squared per second squared, the nuclear stage does not compete favorably with the Centaur plus HFUS at high mission energies. In addition, the Saturn IB - Nuclear(185) - HFUS does not produce significant advantages over the Saturn IB - Centaur - HFUS. The Saturn IB - Nuclear(926) - HFUS performance drops below that of the Saturn IB - Centaur - HFUS. This drop may be explained by looking at the performance curves for the same vehicles without the HFUS. For payloads of greater than about 4630 kilograms, the performance of the Saturn IB-Centaur exceeds that of the Saturn IB-Nuclear(926). The ignition weight of the HFUS is 4825 kilograms plus the payload weight. Thus, for a given payload weight, the HFUS is started at a higher energy on the all-chemical configuration than on the configuration using the nuclear stage.

Figure 12 shows the HFUS of the previous figure replaced by the Burner II. While

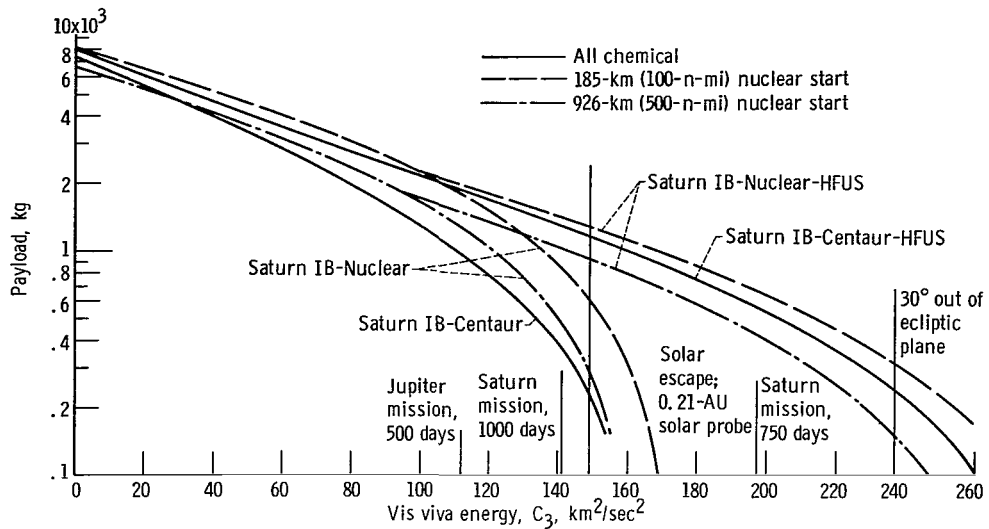


Figure 11. - Effect of adding hydrogen-fluorine upper stage (HFUS) to Centaur and nuclear upper stages on Saturn IB. Reactor power, 300 megawatts.

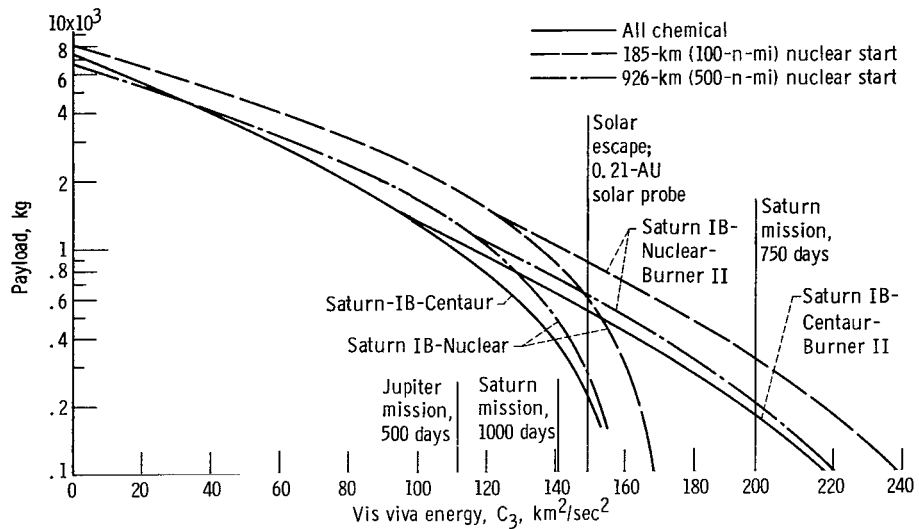


Figure 12. - Effect of adding Burner II to Centaur and nuclear upper stages on Saturn IB. Reactor power, 300 megawatts.

the absolute performance of all three configurations is lower than with the HFUS, the lower ignition weight required by the solid upper stage allows the Saturn IB - Nuclear (185) - Burner II to show a larger advantage over the Saturn IB - Centaur - Burner II. The performance of the Saturn IB - Nuclear(926) - Burner II is comparable to that of the all-chemical vehicle.

On the larger 260-inch solid - S-IVB, the nuclear stage exhibits a greater performance advantage over most of the energy range, as shown in figure 13. Only at high ener-

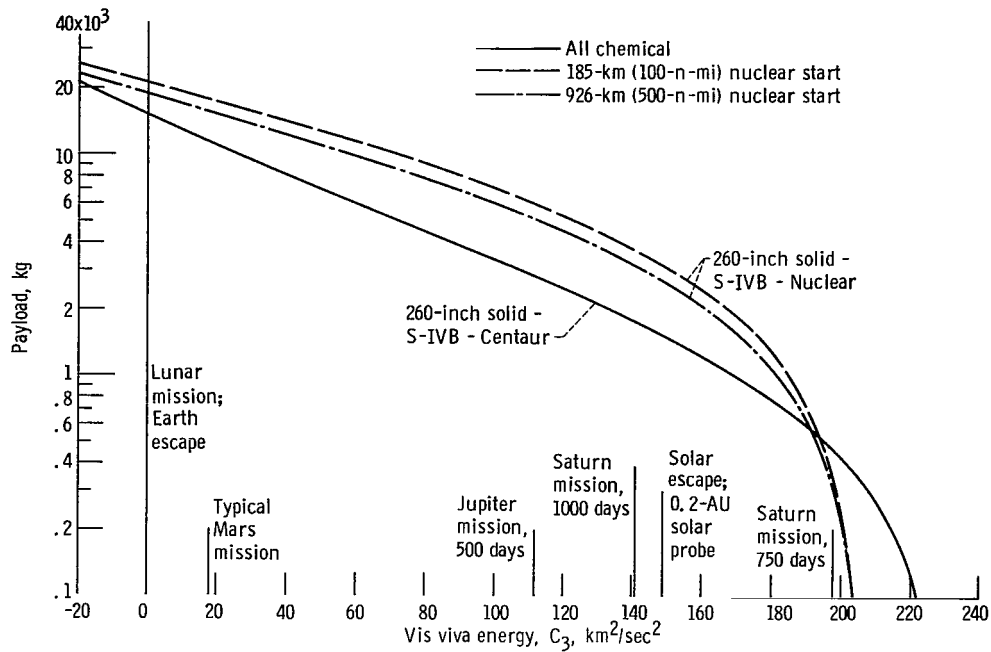


Figure 13. - Comparison of nuclear upper stages with Centaur on 260-inch solid - S-IVB. Reactor power, 600 megawatts at 185 kilometers and 400 megawatts at 926 kilometers.

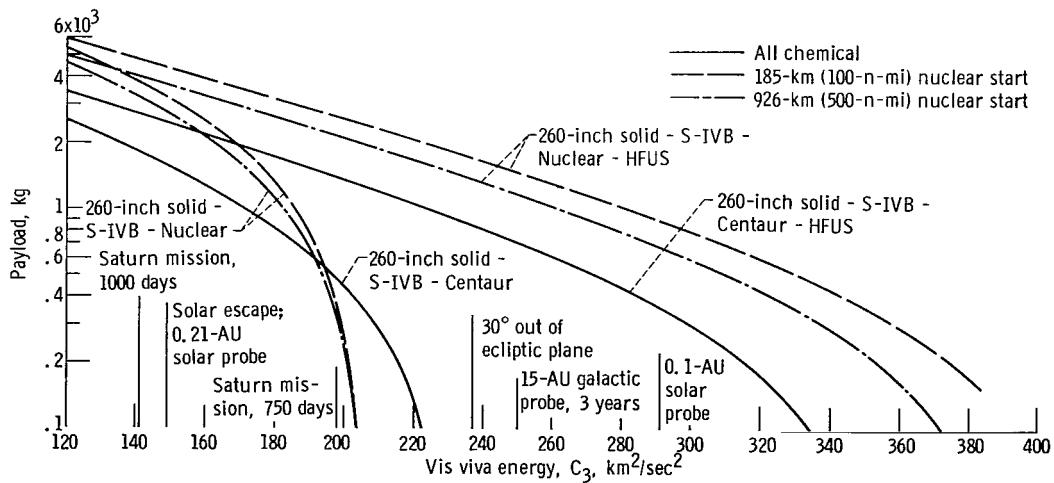


Figure 14. - Effect of adding hydrogen-fluorine upper stage to Centaur and nuclear upper stages on 260-inch solid - S-IVB. Reactor power, 600 megawatts at 185 kilometers, and 400 megawatts at 926 kilometers.

gies can the 260-inch solid - S-IVB - Centaur equal the payloads of the nuclear upper stage starting at either 185 or 926 kilometers. Both nuclear configurations offer sizeable payload gains over the energies required for Jupiter and Saturn missions as well as solar escape and solar probe missions. The 260-inch solid - S-IVB - Centaur, however, can deliver sizeable payloads to the required energies, and the necessary payload weights must determine the value of the performance advantage shown by the nuclear upper stage.

In figure 14, the HFUS has been added to the 260-inch solid - S-IVB - Nuclear vehicles and to the 260-inch solid - S-IVB - Centaur. Only vis viva energies above 120 kilometers squared per second squared are shown. The HFUS extends the capability of both the chemical and nuclear configurations to the high energies required for close solar probes and galactic probes with relatively short trip times. The 260-inch solid - S-IVB vehicle combinations on which the nuclear stage has replaced the Centaur retain their payload advantage when the HFUS is added.

Nuclear-Stage Propellant Requirements

Figures 15 and 16 are presented to illustrate the range of nuclear-stage sizes under consideration and to indicate the running times of these stages. Nuclear-stage propellant weight is shown as a function of vis viva energy in each of these figures. The symbols on

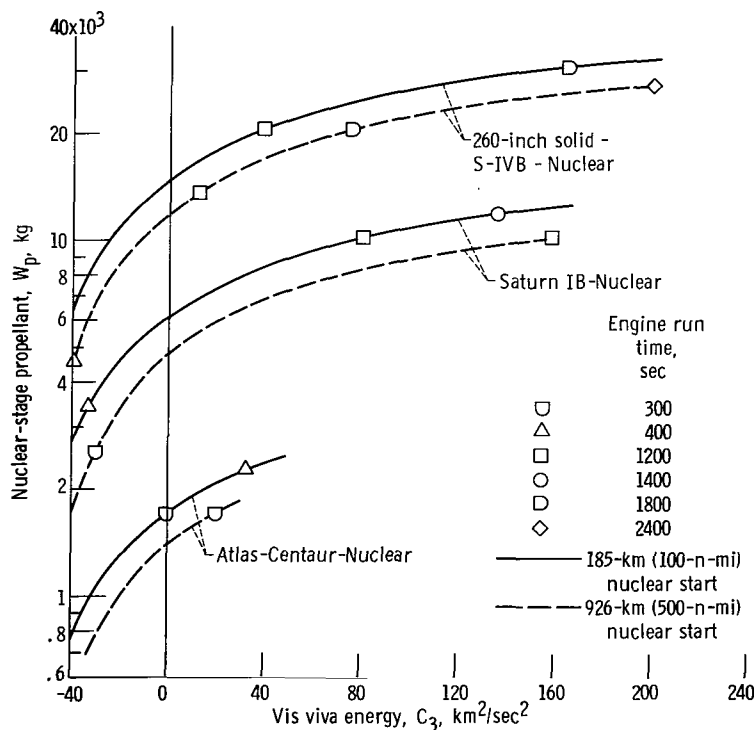


Figure 15. - Nuclear upper stage propellant requirements.

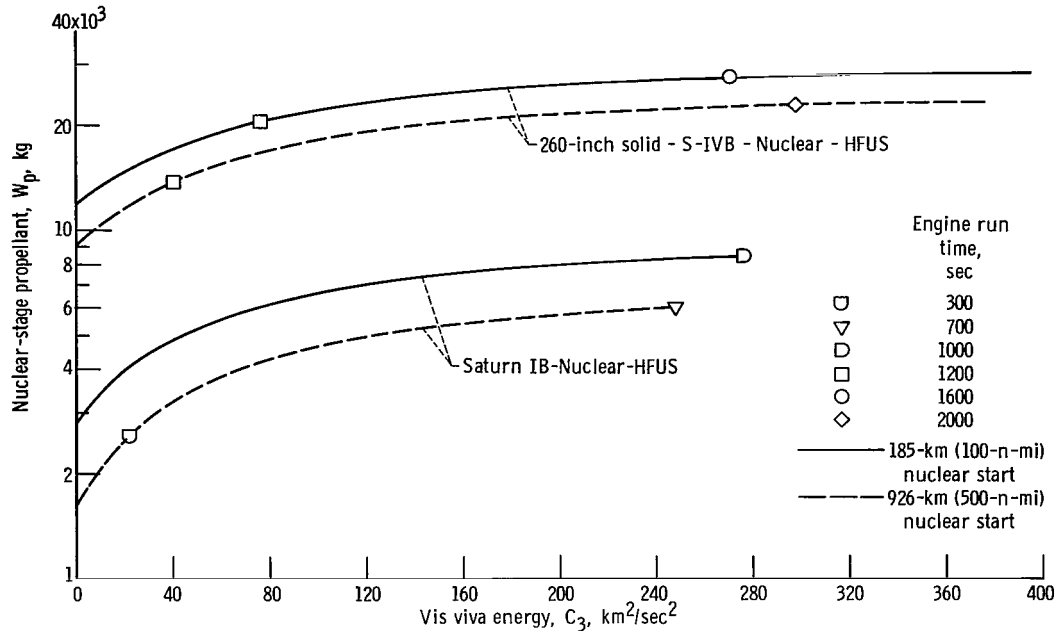


Figure 16. - Nuclear-stage propellant requirements when hydrogen-fluorine upper stage (HFUS) is added.

each curve indicate the nuclear engine running time required at that point on the curve. In figure 15, curves are presented for all three launch vehicles studied with data for both 185- and 926-kilometer circular orbits. The nuclear stage is the final stage in the vehicle configurations used for figure 15. In figure 16, similar data are shown for the Saturn IB - Nuclear and the 260-inch solid - S-IVB - Nuclear vehicles when the hydrogen-fluorine upper stage is added on top of the nuclear stage. The propellant weight shown is for only the nuclear stage; however, the vis viva energy is the burnout energy of the chemical upper stage.

Sensitivity to Nuclear-Stage Hardware Weight Estimate

As indicated in the section Upper-Stage Hardware Weight, the greatest area of doubt in the study involves the assigning of hardware weights to the nuclear stages. Based on the design work involved in the RIFT operational stage, the hardware weight to propellant weight ratio of 0.209 probably represents the lower limit for nuclear stages of the propellant weights being considered herein. Thus, by assuming a constant W_{hw}/W_p of 0.209 throughout the entire propellant range, an optimistic estimate of nuclear-stage performance should be obtained. Figure 17 compares the previously shown performance of the Saturn IB - Nuclear(185) and the 260-inch solid - S-IVB - Nuclear(185) with the

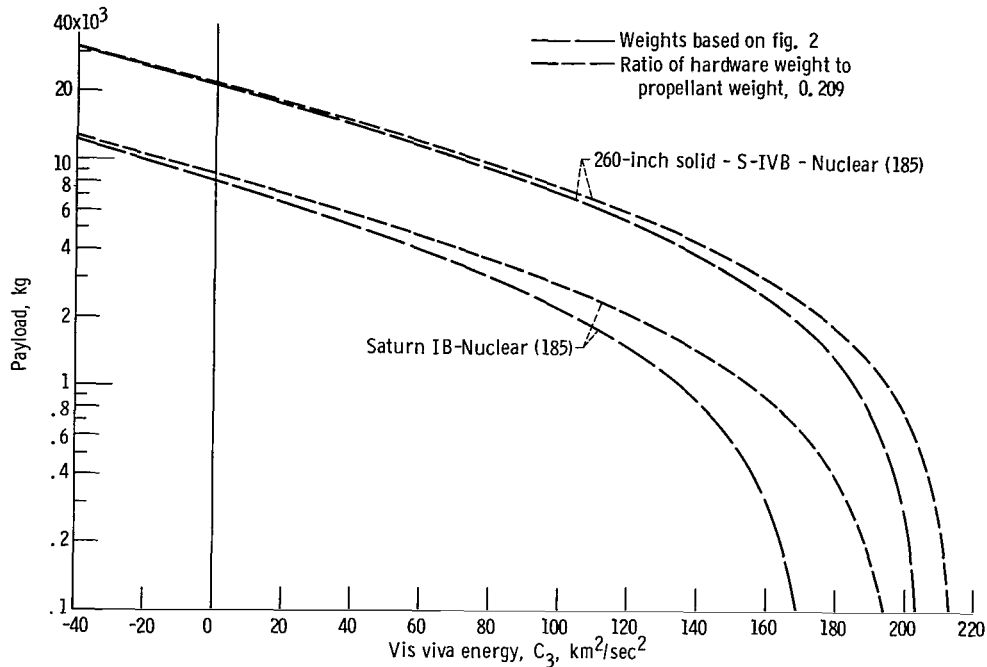


Figure 17. - Effect of hardware weight estimation.

performance of the same vehicle combinations if the hardware to propellant weight ratio is assumed to be constant. While a substantial payload improvement resulted, especially in the Saturn IB, no dramatic change in the payload comparison between chemical and nuclear stages is indicated.

Sensitivity to Approach to Nuclear Propellant Heating

The payload performance curves just considered for the nuclear upper stage employed propellant subcooling with no added weight penalty to counter the nuclear propellant heating. The sensitivity of payload to the treatment of nuclear propellant heating is illustrated in figure 18 by applying the shield mass penalty determined in appendix D. The shield mass penalty was applied to the nuclear third-stage payload performance on the 260-inch solid - S-IVB booster (fig. 13, p. 23) for the 926-kilometer orbital start and the Saturn IB booster (fig. 10, p. 21) for both the 185- and 926-kilometer orbital starts. The original performance curve and that of lower payload due to variable shield mass for the particular reactor power and variable propellant loading are shown in figure 18 for the two boosters.

A payload performance advantage of the Saturn IB - Nuclear configuration for a 185-kilometer orbital start was shown with the propellant subcooling approach to propellant

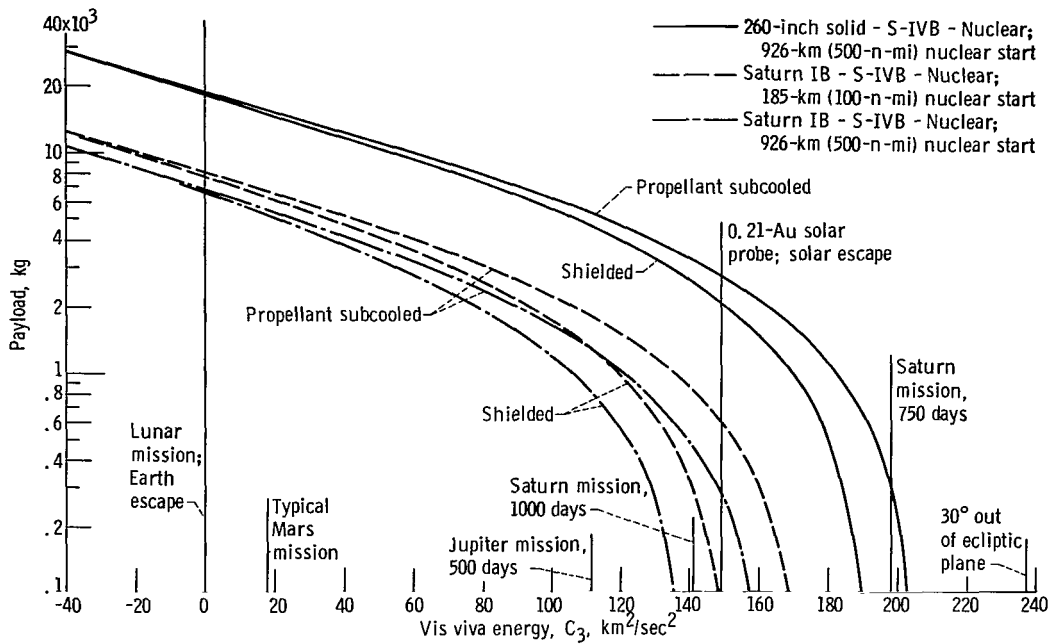


Figure 18. - Effect of shield mass on payload performance.

heating assumed. Use of shielding instead results in loss of the performance advantage when compared with a Centaur third stage. A similar loss of some of the payload advantage occurs for the 260-inch solid launch vehicle. This indicates the importance of propellant subcooling to the nuclear upper stage in the areas of potential performance advantage. The tank pressurization and direct boiloff approaches, as indicated in figure 4 (p. 13), would introduce an intermediate payload reduction compared with shielding for the Saturn IB range of nuclear-stage propellant loading. For the 260-inch solid launch vehicle, the direct boiloff approach is the only intermediate alternative, tank pressurization being unreasonable in the range of propellant loading for those nuclear stages.

CONCLUDING REMARKS

This study was conducted to investigate small-water-graphite-reactor performance when considered in the total nuclear upper stage and compared with chemical upper-stage counterparts. These small-nuclear-rocket stages have potential application as propulsion for a range of possible unmanned missions in the 115- to 13 600-kilogram (250- to 30 000-lb) payload range. The comparison of nuclear and chemical upper stages was therefore made using launch vehicles compatible with this payload range, Atlas-

Centaur, Saturn IB, and 260-inch solid - S-IVB. For reactor weights of 570 to 1020 kilograms over a reactor power range of 200 to 600 megawatts, a corresponding engine weight estimate without shielding of 1290 to 2420 kilograms was developed. To complete the nuclear-stage weight estimate, except for the effects of the radiation environment, the hardware weight estimate varied from 980 kilograms with 2000 kilograms of propellant to 6900 kilograms with 30 000 kilograms of propellant. These estimates are comparable in importance to the nuclear engine weights and, therefore, would justify further study, if more detailed definition of nuclear-stage performance was desired.

The interaction of the nuclear-upper-stage radiation environment with the payload and hydrogen propellant was considered to evaluate the performance penalty. The radiation dose analysis, which accounted for increasing dose rate as the propellant tank empties, indicated that with no shielding the dose to the payload on top of the tank was always within the criteria of 10^6 rads of gamma rays and 10^{13} neutrons per square centimeter of fast neutrons set for radiation damage to electronic components. It was therefore concluded, subject to the accuracy of the payload dose criteria, that any performance penalty for an unmanned mission would be based on propellant heating considerations.

Several approaches were considered to assess the penalty of the radiation environment interaction with propellant heating. These were direct propellant boiloff, propellant subcooling, tank pressurization, and reactor shielding. The propellant subcooling approach, the feasibility of which is still to be determined, is the most desirable since no penalty in boiloff or increased stage jettison weight is incurred. From estimates in this study, propellant loadings of about 20 000 kilograms of hydrogen require subcooling in the range of the hydrogen triple point for the combined nuclear bulk heating and ambient tank wall heating. At about 30 000 kilograms of propellant, a liquid-solid or slush hydrogen mixture of about 20 percent solid hydrogen would be required to provide the necessary heat capacity.

For the payload performance analysis with the various launch vehicles, the propellant subcooling approach was assumed, but the sensitivity of payload to the various other propellant heating approaches was illustrated by consideration of the effect of shielding weight, generally the maximum penalty approach, on the payload. The shield weight required (as much as about 600 kg) was enough to neutralize some areas of potential payload advantage for the nuclear upper stage and indicated the importance of propellant subcooling.

The nuclear-stage payload performance relative to chemical upper stages was examined. Used as fixed chemical upper-stage designs were the presently available Centaur and Burner II and a conceptual hydrogen-fluorine upper stage. Orbital start was assumed for the variable nuclear upper stage. Orbital altitudes of 185 kilometers (100 n mi) and 926 kilometers (500 n mi) were considered to illustrate the effect on payload.

In considering the Atlas launch vehicle, a Centaur upper stage was required in order to place a nuclear third stage, with the smallest water-graphite reactor, in orbit for startup. When compared with the Atlas-Centaur and the Atlas-Centaur with the Burner II or a hydrogen-fluorine stage as a third stage, the nuclear stage was not competitive and was not considered further.

For the Saturn IB and 260-inch solid launch vehicles, the nuclear engine thrust was optimized for the competing effects of the nuclear engine mass increase with thrust and the increased "gravity loss" of longer operating times at lower thrusts. A 300-megawatt water-graphite reactor (i. e., 6.67×10^4 -N or 15 000-lb thrust) was optimum for the Saturn IB at 185- and 926-kilometer starting orbits, whereas 600- and 400-megawatt water-graphite reactors were optimum for the 260-inch solid launch vehicle at 185- and 926-kilometer orbits, respectively.

Considering the performance of these two launch vehicles relative to chemical upper stages and typical unmanned missions, the following areas of potential usefulness of the nuclear upper stage were defined subject to the accuracy of the nuclear stage and engine weight estimates. For the Saturn IB launch vehicle, a nuclear stage started from a 926-kilometer orbit showed comparable performance to the Saturn IB-Centaur, while for a 185-kilometer orbit, a significant payload improvement was indicated. The effect of safety considerations on choice of orbital start altitude is therefore of major importance to the nuclear-stage payload performance in this case. The Saturn IB - Nuclear configuration offers a payload improvement for the typical Jupiter and Saturn mission energies and more than doubles the payload for a solar escape mission or a 0.21-astronomical-unit solar probe. Addition of chemical fourth stages to the Centaur and nuclear third stages resulted in nearly equal performance for both the chemical and nuclear configurations at the resultant higher mission energies.

The nuclear third stage on the larger 260-inch solid - S-IVB exhibited a larger performance advantage over the Centaur third stage throughout most of the mission energy range. Both orbital altitudes of nuclear start considered showed the significant performance advantage, thereby indicating that safety considerations have a lesser effect in this case. Typical Jupiter, Saturn, solar escape, and solar probe missions show the large payload improvement. However, this gain must be weighed against actual payload requirements for the various missions since the Centaur third stage can deliver sizeable, although lower, payloads. Addition of the chemical fourth stage extends the capability of both the chemical and nuclear configurations to very high energies making close solar probes and ambitious galactic probes possible. The nuclear configurations for both orbital start altitudes retained the former payload advantage at these higher mission energies when the chemical fourth stage was added.

A cross-comparison of a booster - nuclear-third-stage combination with a booster plus chemical third and fourth stages can also be made. This comparison shows that the

advantage of chemical rocket staging to one more level outweighs the higher specific impulse advantage of the nuclear third stage, if lower payloads at higher mission energies are required.

The payload performance aspects of the study have indicated that nuclear upper stages restricted to orbital start and employing potentially the smallest graphite nuclear rocket reactor, namely, a water-graphite reactor of small critical size, along with propellant subcooling require launch vehicles of at least the size of the Saturn IB in order to show a payload advantage for unmanned missions. Furthermore, a reactor power of 400 to 600 megawatts seems more appropriate than the smallest size (approximately 200 MW) for unmanned missions.

Lewis Research Center,
National Aeronautics and Space Administration,
Cleveland, Ohio, May 31, 1968,
120-27-06-18-22.

APPENDIX A

DETAILS OF ENGINE COMPONENT WEIGHT ESTIMATE

Pressure Vessel

An equation from reference 6 was used to calculate for any reactor size the weight of the titanium cylindrical shell and the hemispherical dome with allowance for flanges, dome reinforcement, bolts, gaskets, and so forth. The thickness is determined from an allowable yield stress of 46 900 newtons per square centimeter (68 100 psi) and a typical 448-newton-per-square-centimeter (650-psia) internal pressure of the water coolant in the dome and radial reflector regions. The calculated pressure vessel weight curve for several water-graphite reactors was faired into the NERVA value to provide the estimate over the full power range, as shown in table I (p. 5). The weight equation has been shown, in reference 6, to give good agreement with the NERVA pressure vessel weight.

Nozzle

A nozzle weight estimate for the power range of small nuclear rockets was related to the nozzle weight equations derived in reference 6. The series of equations for the four major nozzle components was derived for the study of NERVA reactors of higher power (~5000 MW). Values for normalization constants and allowable nozzle tube and jacket hoop stresses were obtained by comparing the equations with detailed design data obtained from Aerojet-General Corporation.

The NERVA nozzle weight of 348 kilograms was calculated as 390 kilograms with these equations when using the temperatures, pressures, and flow rates from reference 4 (pp. II-6, II-7, and II-8) and expansion ratios, material densities, coolant tube diameter, throat section length, plenum section length, and skirt wall thickness from reference 6 (p. I-20). Another detailed nozzle design of 136 kilograms weight at 240 megawatts reactor power was calculated to be 116 kilograms when the same parameters were used except for the following values from an Aerojet nozzle design analysis for a small nuclear rocket (SNR):

- (1) Nozzle coolant inlet pressure, P_i , 672 newtons per square centimeter (975 psia)
- (2) Nozzle chamber pressure, P_c , 344 newtons per square centimeter (500 psia)
- (3) Nozzle chamber temperature, T_c , 2500 K (4500° R)
- (4) Divergent section expansion ratio at which cooling begins, ϵ_d , 33
- (5) Divergent section expansion ratio at which jacket ends, $\epsilon_{d,j}$, 9

(6) Overall nozzle expansion ratio, ϵ_m , 100

(7) Nozzle throat propellant mass flow rate, \dot{w}_h , 6.8 kilograms per second (15 lb/sec)

(8) Nozzle coolant mass flow rate, \dot{w}_c , 3.4 kilograms per second (7.5 lb/sec)

The nozzle expansion ratio parameter has a major effect on nozzle weight, and no curve for a single nozzle expansion ratio will interpolate between the two detailed design points, as shown in figure 19. A linear variation of nozzle weight was therefore assumed, as shown by the dashed curve. The selected end point at 385 kilograms and 1000 megawatts power was offset from the NERVA data point to account for the different T_c , P_c , and P_i typical of the SNR. The dashed curve indicates a reduction in nozzle expansion ratio and, hence, specific impulse with increasing reactor power. In this SNR study, however,

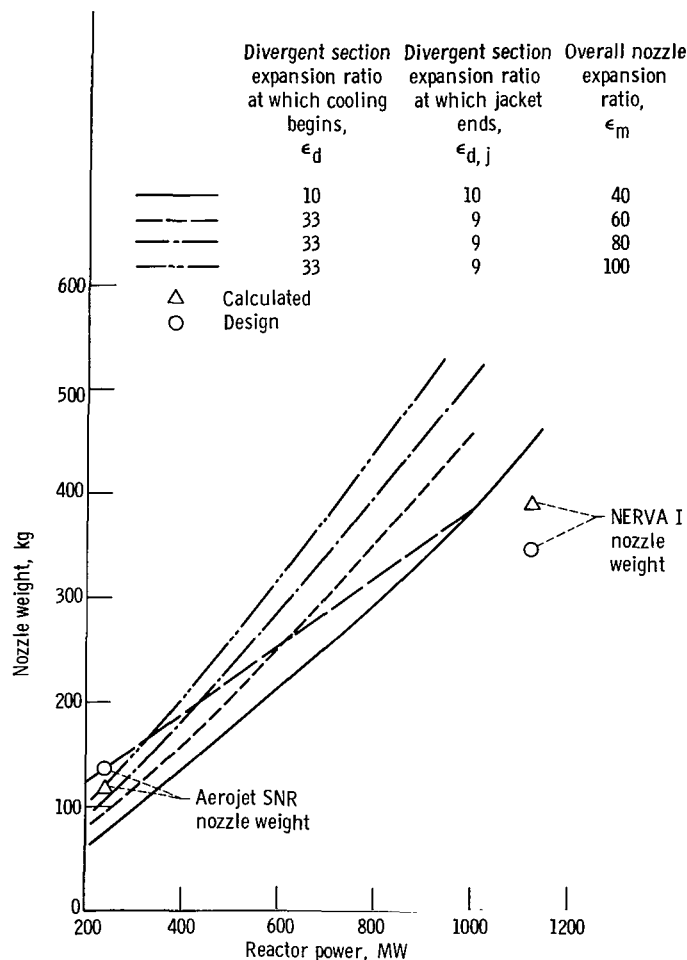


Figure 19. - Nozzle weight as function of reactor power. Nozzle chamber temperature, 2500 K; nozzle chamber pressure, 344 newtons per square centimeter (500 psia); nozzle coolant inlet pressure, 672 newtons per square centimeter (975 psia).

a conservative and constant specific impulse of 7850 newton-seconds per kilogram (800 lb force-sec/lb mass) has been assumed over the whole reactor power range.

Propellant and Water Turbopump Assemblies

While the turbopump weight equation from reference 6 (p. VII-28) gave very good agreement with the NERVA bleed cycle design (ref. 4, p. II-2) application to the SNR flow rate and discharge pressure at 240 megawatts reactor power, with either bleed or topping cycle, substantially underestimated the weight. The latter weight estimate of 79.3 kilograms from an Aerojet detailed design was about 56.6 kilograms heavier than the equation estimate. A linear relation between the two detailed design points was therefore assumed for the values in table I (p. 5) and is supported by the linearity of the turbopump weight equation.

The water turbopump assembly weight was obtained from the hydrogen turbopump weights by assuming that pump weight is proportional to pump discharge pressure and to volumetric flow rate to the $3/2$ power (ref. 29, p. 52). For a 254-megawatt water-graphite reactor design, the ratio of water to hydrogen turbopump weights is 0.252, and this factor was used over the full reactor power range.

Remaining Engine Weight Components

For flow-line and tank valve assemblies, upper and lower thrust structures and thrust vector structure, diagnostic instrumentation system, engine control system, and engine pneumatic system, a linear variation generally between two data points from the NERVA (ref. 4) and the Aerojet SNR engine component weights at 240 megawatts power was used. An exception was made in the allowance for additional piping and heat-exchanger weight of a second flow loop for the water moderator - coolant. Weight estimates for both the hydrogen and water flow systems of water-moderated tungsten nuclear rockets (see example, ref. 2), which have similar flow systems and pressure levels, were used. These weights were converted on the basis of water flow rate (assuming the water loop is the major weight contribution) to the water-graphite reactor flow system and represent an average of 140 kilograms weight increase for the water loop compared with the NERVA and Aerojet SNR data points generally used.

In addition, the Lockheed modified thrust structure weight of reference 8 (pp. A-10 and B-2) for NERVA was scaled to lower reactor powers by assuming the weight to be proportional to compressive load during thrusting. Also, a tank pressurization component was subtracted from the NERVA pneumatic system weight to correspond to engine pneumatic system only.

APPENDIX B

PAYLOAD RADIATION LEVELS FOR UNMANNED MISSIONS

The calculation of time-integrated dose at the payload takes into account the changing propellant volume between the reactor and payload. The calculation was performed for the maximum propellant load of 44 000 kilograms of liquid hydrogen considered in this study and then generalized to the full range of propellant mass. The 44 000 kilograms of liquid hydrogen corresponds to the propellant requirement for the 432-megawatt reactor design, the largest of the three reactors considered in the radiation environment analysis, and to the maximum 60-minute run time typical of the graphite-fuel-element reactor type. The receiver point in this case is 24.4 meters from the top of the core.

The cumulative fast-neutron and gamma-ray doses for a fixed separation distance of

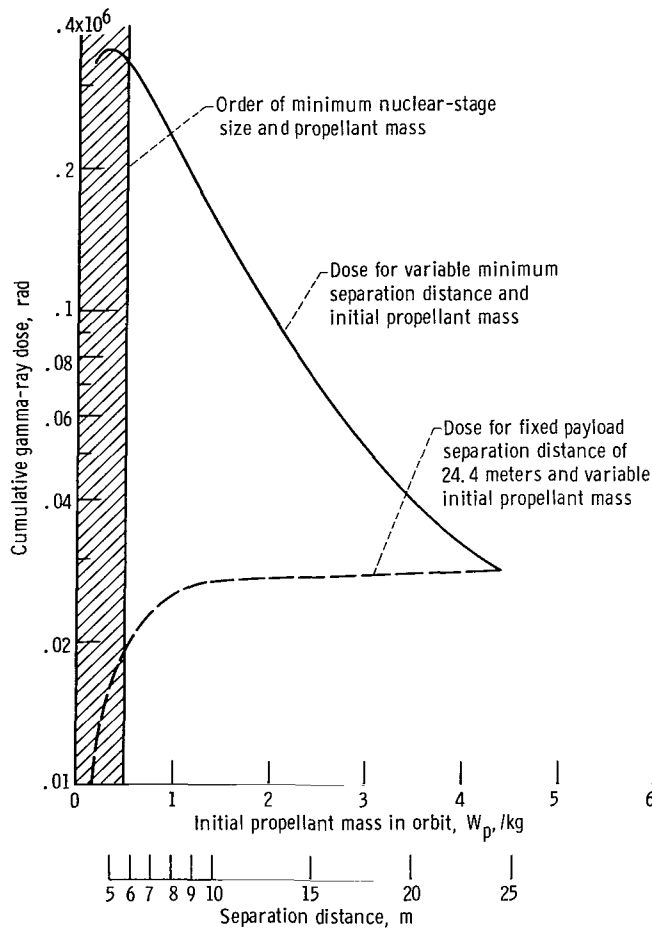


Figure 20. - Cumulative gamma-ray dose at payload independent of reactor power for constant 6.0-meter tank diameter, no shielding.

about 24.4 meters, but variable tank height and intervening initial propellant load, are shown as the dashed curves in figures 20 and 21. These accumulated dose values are independent of reactor power level and corresponding propellant flow rate since the exposure time, or time to empty the tank, is inversely proportional to the power. At the lower propellant masses, especially in the gamma dose case, the dose increases with propellant mass additions because the engine run time, and, hence, radiation exposure time, is longer and some of the radiation is still penetrating the successive mass additions. Beyond about 15 000 kilograms of hydrogen for gamma radiation and only about 1000 kilograms for fast-neutron radiation, however, the radiation penetration is initially negligible as the tank drains, and no further increase of dose occurs.

The fixed separation distance for the dashed curves in figures 20 and 21 puts the payload directly above the tank only for the 44 000-kilogram propellant loading. However,

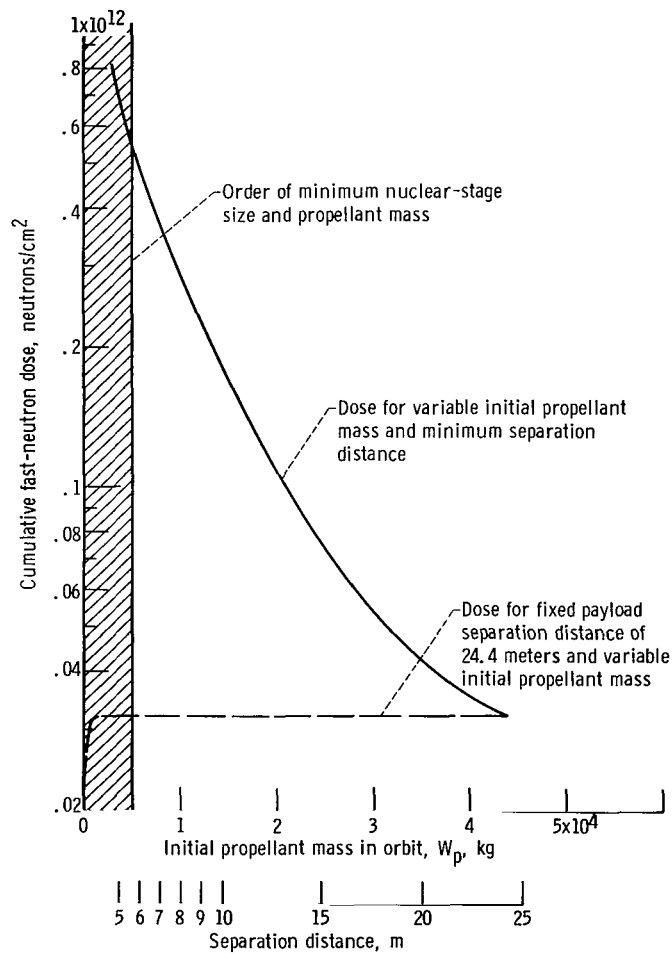


Figure 21. - Cumulative fast-neutron dose at payload independent of reactor power for constant 6.0-meter tank diameter, no shielding.

direct earth launch and subsequent nuclear-stage startup in orbit implies location of the payload directly above the tank for all propellant loadings. The solid curves in figures 20 and 21 represent this latter situation, the accumulated dose with the variable minimum separation distance for all propellant loadings. These curves were obtained from the dashed curves by applying a $1/R^2$ geometrical attenuation correction based on the separation distances. The difference between the curves illustrates the degree of dose reduction that results from extra separation at the lower propellant masses.

APPENDIX C

DETAILS OF RADIATION DOSE AND PROPELLANT HEATING CALCULATIONS

For computation purposes, the reactor assembly was represented as shown in figure 22. The composition of each region is listed in table IV. Relative power distributions in the axial and radial directions were obtained using the 1-D Sn transport code

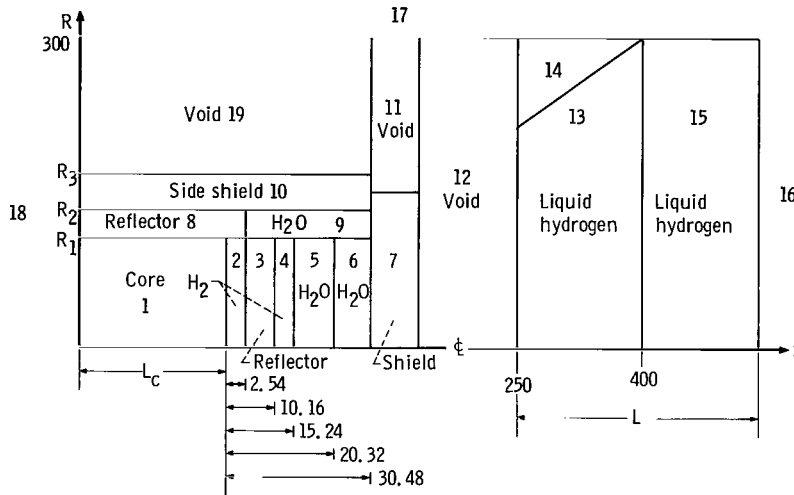


Figure 22. - Model of reactor shield - propellant tank configuration used in QADHD calculations. (All dimensions in cm; not to scale; numbers denote QAD regions.)

TABLE IV. - COMPOSITION REGIONS

Reactor component	QADHD region	Density, g/cm ³								
		H	C	O	Ni	Nb	U	Be	Al	Total
Core	1	0.0144	1.044	0.115	0.077	0.07	0.31	0	0	1.63
Radial reflector	8	.011	0	.089	0	0	0	1.67	0	1.77
Water	9, 6	.111	0	.889	0	0	0	0	0	1.0
Axial reflector	3	.0144	0	.115	.083	0	0	1.435	0	1.647
Hydrogen	2, 4	0	0	0	.083	0	0	0	0	.083
Water	5	.110	0	.880	.083	0	0	0	0	1.073
Void	11, 12, 14, 16, 17, 18, 19	0	0	0	0	0	0	0	0	0
Shield	7, 10	0	0	0	0	0	0	0	2.7	2.7
Liquid hydrogen	13, 15	.0714	0	0	0	0	0	0	0	.0714

DTF-IV (ref. 30). In addition to the power (fission) density, the number and distribution of secondary gamma-producing neutron capture events were determined in the reactor assembly.

Radiation dose rates and propellant heating were calculated by using the point-kernel, line-of-sight code QADHD (ref. 12). This code uses infinite-medium buildup factors for gamma rays and the Albert-Welton kernel to estimate the fast-neutron dose. The gamma source spectrum used is listed in table V and is composed of 7.2 MeV per fission from

TABLE V. - CORE GAMMA SPECTRUM

Group	Energy range for group, MeV	Source strength, MeV/fission
1	0.1 to 0.4	1.205
2	0.4 to 0.9	3.560
3	0.9 to 1.35	2.520
4	1.35 to 1.8	1.970
5	1.8 to 2.2	1.435
6	2.2 to 2.6	1.134
7	2.6 to 3.0	.857
8	3.0 to 3.5	.760
9	3.5 to 4.0	.577
10	4.0 to 4.5	.365
11	4.5 to 5.0	.219
12	5.0 to 5.5	.129
13	5.5 to 10.0	.117
Total		14.848

prompt fission gamma rays, 6.2 MeV per fission from decay gammas (attained after 60 min of reactor operation), and a total of 1.44 MeV per fission from capture gammas in all core materials, for a total of 14.8 MeV per fission. The contribution to heating from capture gammas produced in other regions of the reactor assembly was estimated to be small (less than 10 percent) compared with the contribution from core gammas.

The tank bottom is assumed to be about 2.5 meters from the top surface of the reactor core, and the tank is represented as a truncated 45° conical bottom section of 1.5 meter height below a cylindrical section of 6.0 meters in diameter and variable height (depending on the propellant loading of the stage design).

In figure 22, certain dimensions (R_1 , R_2 , L_c , and L) are not specified. These depend on the reactor power level (the three reactors considered for 181, 254, and 432 megawatts power are of different core diameter and radial reflector thickness) and total

quantity of propellant in the tank. The parameters, R_1 , R_2 , and L_c , are listed in reference 5 for classification reasons. The parameter L is specified as follows.

Reactor power, MW	Length, L, cm	Operating time, min
181	288	15
	512	30
	955	60
254	378	15
	690	30
	1315	60
432	595	15
	1130	30
	2230	60

The flow rate of liquid hydrogen propellant per megawatt of thermal reactor power was taken to be

$$\frac{\dot{W}}{P} = 0.0284 \text{ kg}/(\text{sec})(\text{MW})$$

where

\dot{W} mass flow rate, kg/sec

P reactor thermal power, MW

This flow rate corresponds to the assumed specific impulse for the small water-graphite nuclear rockets of 7840 newtons per kilogram per second (800 lb force/(lb mass)(sec)) and assumes the engine to be capable of developing 222.4 newtons thrust per megawatt of reactor thermal power. The flow rates for the three reactors considered are shown in the following table.

Thermal power, MW	Thrust, N	Propellant flow rate, kg/sec
181	40 200	5.14
254	56 500	7.21
432	96 000	12.3

The curves showing final propellant temperature rise of any given engine run time were constructed from propellant temperature rise histories calculated by QADHD for each reactor-shield system operating for 3600 seconds, or 60 minutes.

The temperature rise at any time t multiplied by ρC_p (density and specific heat, respectively) represents the stored energy per unit volume in the propellant at that time by virtue of the complete-mix model. It can be shown that the temperature rise, corresponding to any run time equal to $3600 - t$, is given by $\Delta T = T(3600) - T(t)$ read from a QADHD temperature rise history for 3600 seconds and represents the temperature rise of the shorter run time ($3600 \text{ sec} - t$) and its lower initial propellant mass. Figure 23 illustrates the typical shape of the temperature histories for a QADHD calculation, in this case with a 50-gram-per-square-centimeter reactor-diameter, shadow shield and 3600 seconds of engine operation.

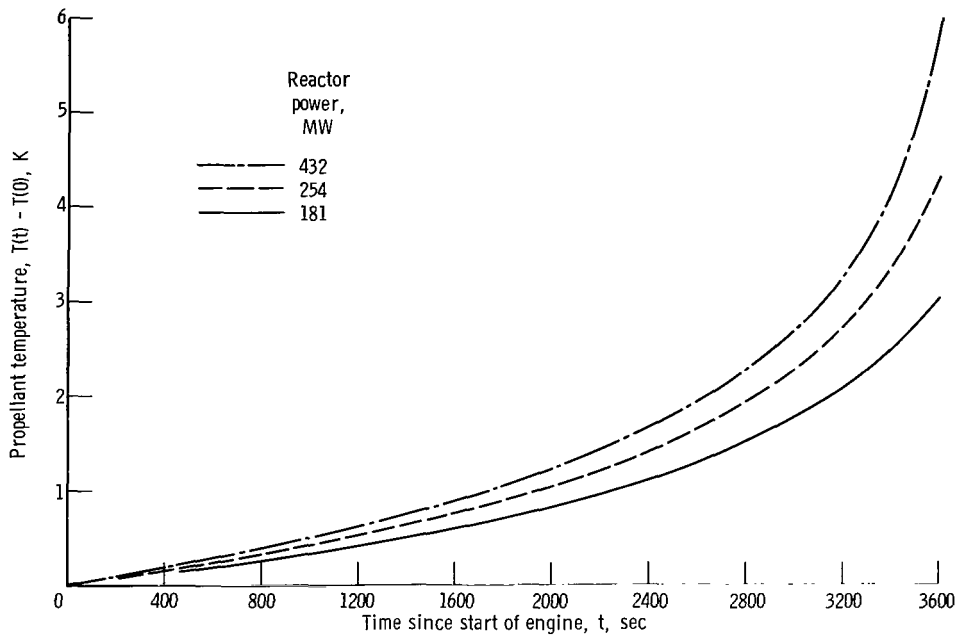


Figure 23. - Propellant temperature rise against time since start of engine operation. Engine run time, 3600 seconds; 50-gram-per-square-centimeter reactor-diameter shadow shield; complete-mixing model.

APPENDIX D

NUCLEAR HEATING OF PROPELLANT

The propellant heating during the nuclear engine run time consists primarily of the nuclear bulk propellant heating. A small propellant heating component from nuclear wall heating was neglected. Some additional heating through the insulation and tank walls also occurs from the space environment and was considered in order to illustrate the relative magnitude of this nonnuclear heating component.

The space environment propellant heating can be estimated by assuming propellant heat flux values through typical tank insulation. From reference 31 a heat flux of 295 watts per square meter is representative of sealed-foam constrictive-wrapped, external insulation 1.016 centimeters (0.4 in.) thick. The foam insulation is typical of the type used for the Centaur, Saturn S-II, and Saturn S-IVB stages, where it is employed as external jettisonable, external nonjettisonable, and internal insulation, respectively, (ref. 31, p. 12). An alternate insulation has been proposed as part of a more advanced overall tank design for the larger NERVA engine type of nuclear stage (ref. 32). This design may produce a substantially lower heat flux to the propellant of 0.79 watt per square meter in the space vacuum environment. A multilayer, thin reflective foil insulation (2.54 cm thick) is used in conjunction with a nonintegral tank design. In this design the outer primary load-carrying structure, including the insulation, is separated from the inner unstiffened tank wall by a vented space (vacuum at orbital conditions).

When the possible range of heat flux was defined in this way, the boiloff due to space environment heating was based on the high value. The lower limit resulted in a negligible boiloff contribution compared with the nuclear bulk heating. The tank heat-transfer area assumed for the heat flux is the conical bottom surface area and sidewall area up to the liquid height. The tank is 6 meters in diameter with a truncated 45° conical bottom of 1.5 meter height.

The nuclear bulk heating of the propellant results from gamma-ray and fast-neutron interactions with the hydrogen as the propellant tank empties. The nuclear heating rate spatial variation in the propellant was evaluated by using the computer program QADHD (ref. 12). Further details of the calculation and geometry are given in appendix C. Typical radially averaged heating rates along the axis of the tank are shown in figure 24 for the 432-megawatt reactor power. The figure shows that the heating is concentrated near the bottom of the propellant tank because of attenuation of the gamma and fast-neutron radiation by the propellant. The integrated gamma-ray heating rate over the full propellant depth represents about 91 percent of the total nuclear heating rate.

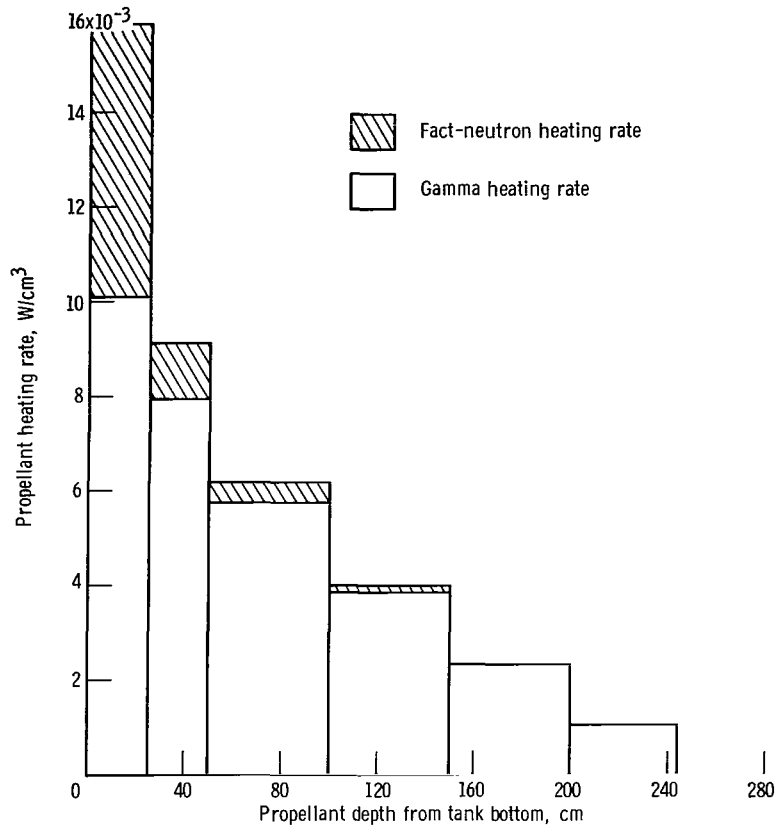


Figure 24. - Nuclear bulk heating of propellant, radially averaged local axial heating rates for 6-meter-diameter tank with truncated conical bottom. Reactor power, 432 megawatts.

Direct Propellant Boiloff Approach

Complete mixing of both the nuclear and wall heat inputs with the total propellant is assumed to be caused by the turbulent bulk mixing of the nuclear heating. Figure 25 shows the amount of propellant boiloff resulting from these heat inputs. This boiloff estimate represents the boiloff after utilizing the small propellant subcooling heat capacity due to a typical tank design pressure of 17.2 newtons per square centimeter (25 psia) and a propellant supply temperature of 20.4 K. The nuclear propellant heating values used were time-integrated as the tank empties and propellant volume decreases.

The abscissa of figure 25 represents a variable total running time of the nuclear rocket up to 1 hour and defines for each reactor power a variable initial propellant loading as shown by the lines of constant propellant weight. This initial propellant loading W_p is the useable propellant in orbit at nuclear engine start, and the boiloff estimates of figure 25 must be added to obtain the total initial loading in orbit for the direct boiloff approach.

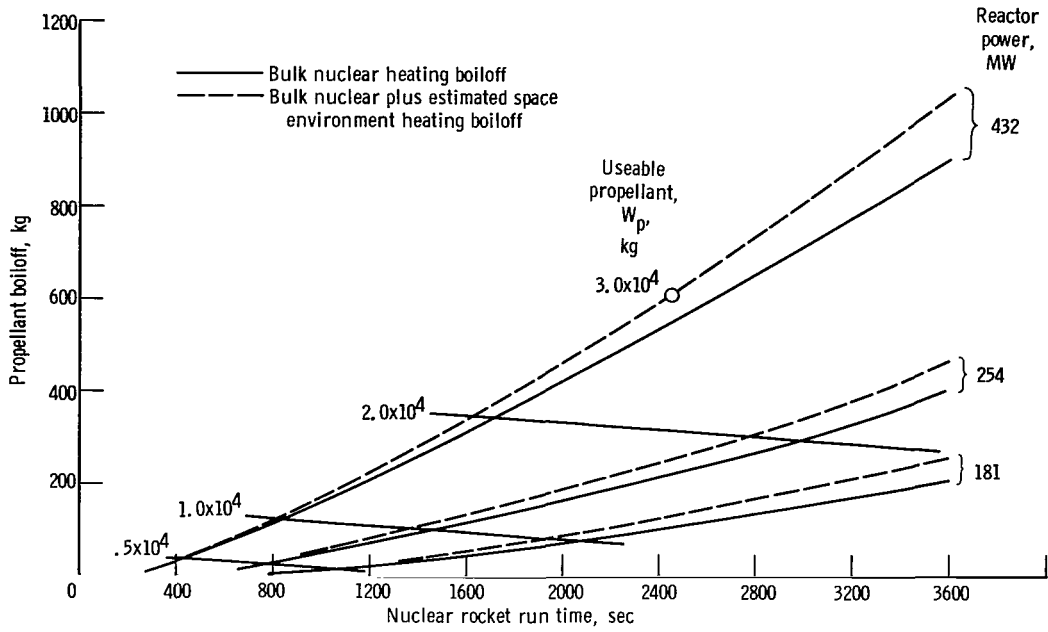


Figure 25. - Propellant boiloff mass penalty. Heat of vaporization, 4.46×10^5 joules per kilogram.

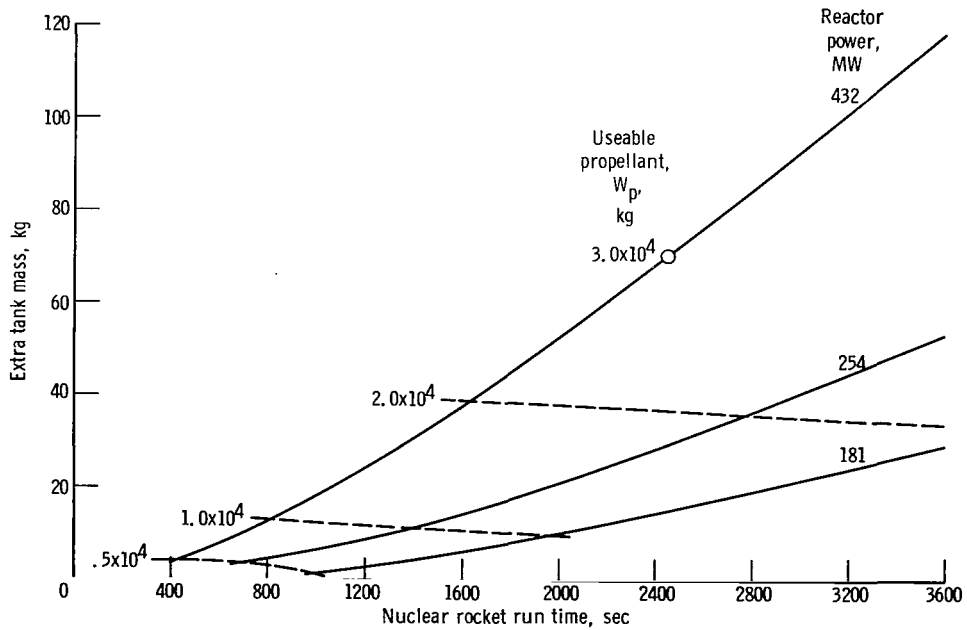


Figure 26. - Tank mass penalty for direct propellant boiloff approach.

Extra tank weight (including insulation) to contain the additional propellant for boiloff is the other part of the weight penalty. The increased tank weight was estimated by using the value of 0.1138 kilogram of tank (including insulation) mass per kilogram of additional propellant weight. This value was obtained from unpublished tank weight data in a Douglas Aircraft Company preliminary study of several nuclear-stage sizes based on modification of S-IVB stage design. The extra tank mass for the same range of nuclear rocket run time and reactor powers as given for the propellant boiloff is shown in figure 26.

Propellant Subcooling Approach

The boiloff weight penalty of the nuclear heating phase can be eliminated by using a subcooled propellant supply at the 17.2-newton-per-square-centimeter typical tank design pressure to absorb the heat input. This approach results in no relative weight pen-

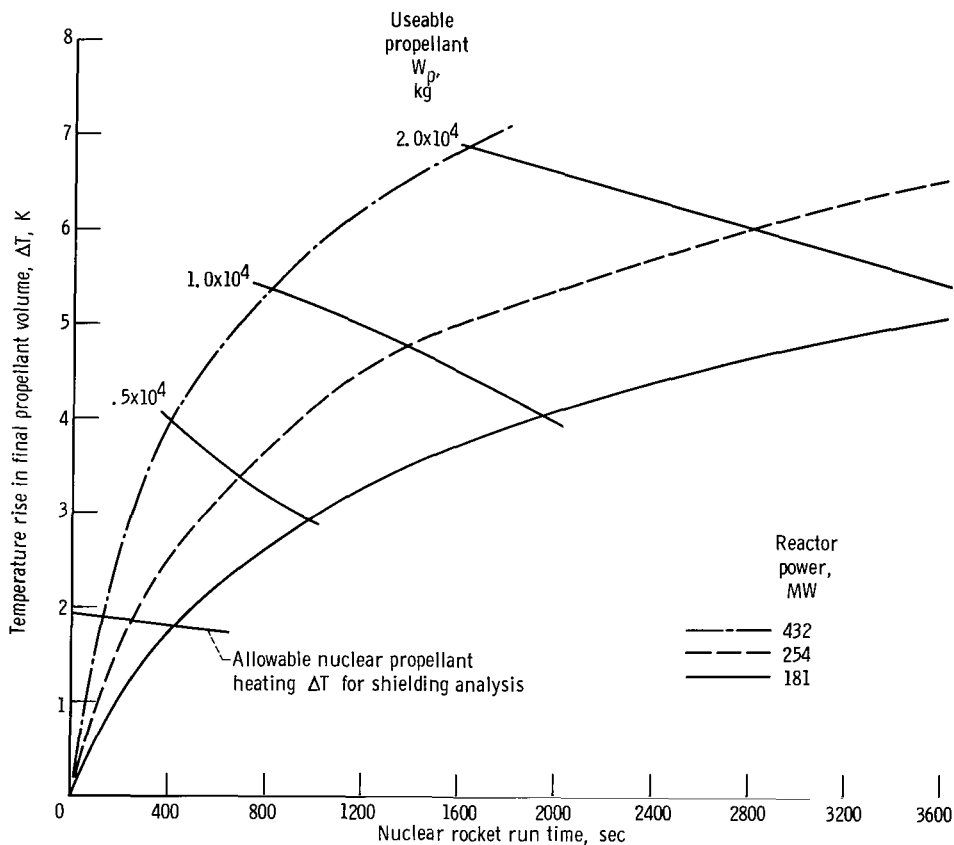


Figure 27. - Nuclear bulk heating propellant temperature rise. No shielding; tank diameter, 6 meters; constant specific heat, 9.41×10^3 joules per kilogram per K.

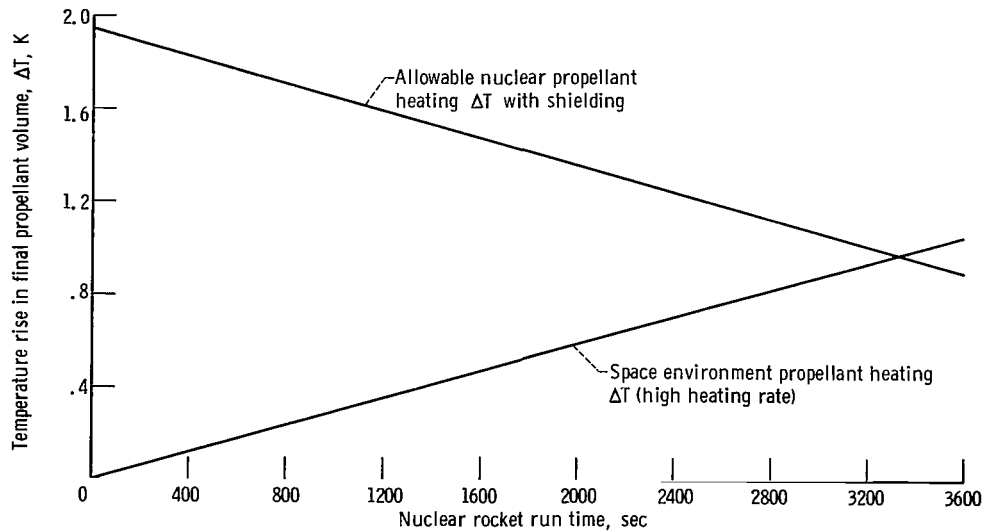


Figure 28. - Space environment heating and nominal propellant subcooling for shielded propellant heating. Constant specific heat, 9.41×10^3 joules per kilogram per K.

ality since the initial propellant mass is preserved, and no greater pressurization than usual is required. For this case, the degree of subcooling required to compensate for the heat input was determined in order to illustrate the magnitude and variation of subcooling with reactor power and run time.

From calculations of the nuclear bulk propellant heating for the unshielded reactor-tank geometries (see appendix C), the propellant temperature rise (proportional to heating per unit propellant mass) of the last volume of propellant in the tank was obtained as a function of reactor power and run time (fig. 27). The ΔT for complete mixing of the space environment heat input (fig. 28) was added to these values, and the total ΔT was corrected for average specific heat over the temperature changes. (The additional curve in figs. 27 and 28 for "allowable nuclear propellant heating ΔT " is explained later in the section Reactor Shielding Approach.) The variation in required number of degrees of subcooling for liquid saturation and a zero NPSP condition at the end of run time was obtained, as shown in figure 29.

The longer run times, with approximately 20 000 kilograms of propellant, employ all the subcooling available between the saturation temperature at a 17.2-newton-per-square-centimeter tank design pressure and the hydrogen triple point at 14 K. However, useful propellant loadings of as much as 30 000 kilograms of hydrogen are possible for a small-nuclear-rocket stage from the payload performance analysis. Extension of the 432-megawatt-reactor run time and propellant loading to this range in figure 29 (about 2400 sec run time) would require a liquid-solid mixture, or slush hydrogen mixture, of about 20 percent solid hydrogen. Studies of the properties and the storage and transport

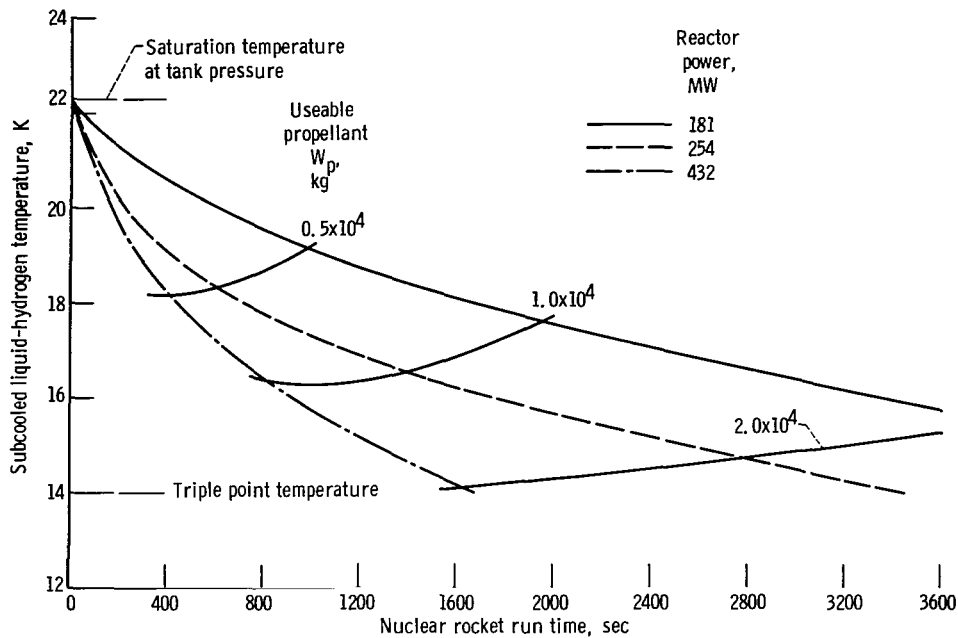


Figure 29. - Propellant subcooling requirement. Zero NPSP at end of run time.

characteristics of slush and subcooled hydrogen for such an application have been reported (refs. 18 and 19) and are in progress (refs. 20 and 21). While no insurmountable problems have thus far been uncovered, an operational system of this type is not a foregone conclusion at this time.

Tank Pressurization Approach

The boiloff weight penalty of the nuclear propellant heating phase can also be eliminated by raising the tank design pressure above the typical 17.2 newtons per square centimeter to achieve adequate subcooling for the heat input. The assumptions and approach are the same as those for propellant subcooling at the typical tank pressure. Neglecting any changes in pressurization system weight as being minor, the weight penalty in this case is the increased tank weight (including insulation) required for a higher tank pressure but the same useable propellant weight as for the no-propellant-heating base case.

The higher tank design pressures, equivalent to the vapor pressure at the final propellant temperature, were determined from the nuclear bulk heating propellant temperature rise data of figure 27 (corrected for average specific heat of the temperature rise). The additional increment of temperature rise in the final volume of propellant at liquid exhaustion due to complete mixing of the space environment wall heating was also in-

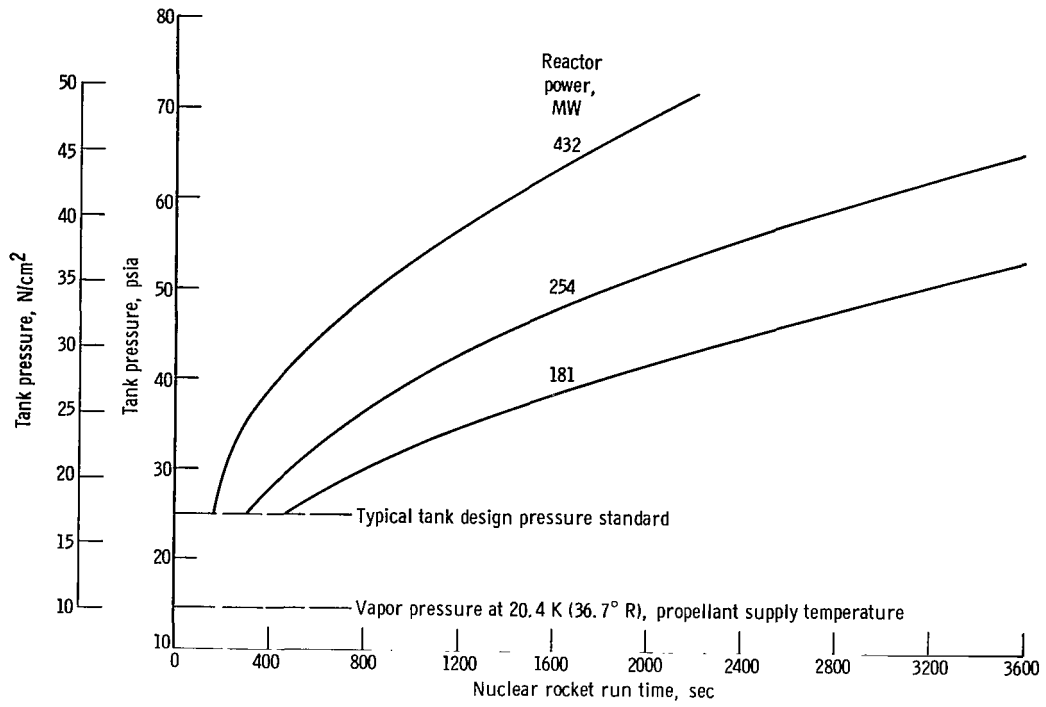


Figure 30. - Tank design pressure for tank pressurization approach. Zero NPSP at end of run time.

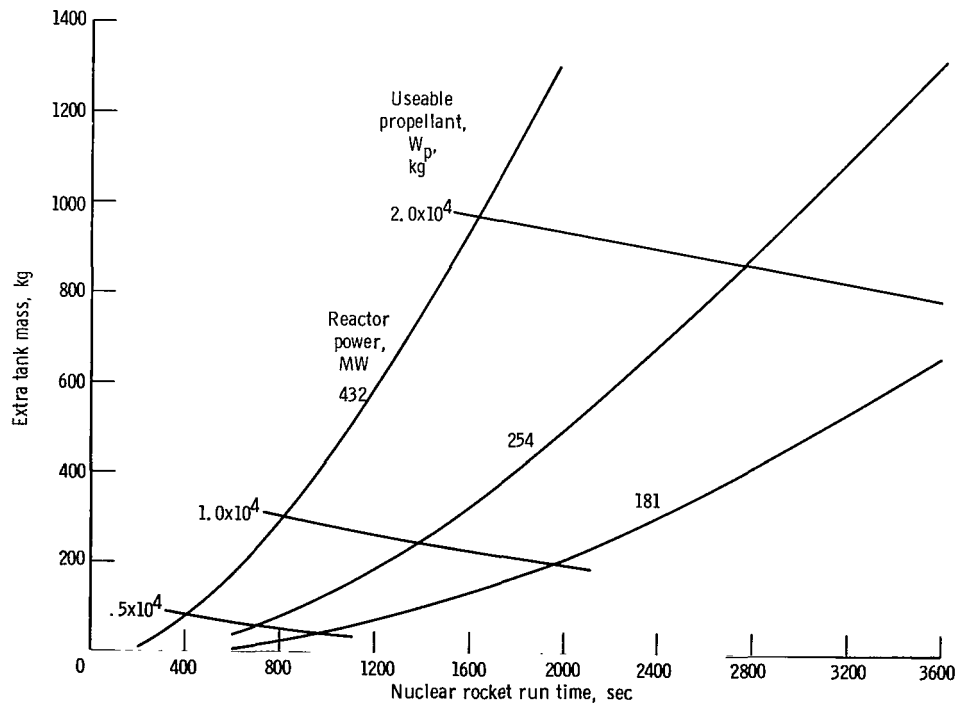


Figure 31. - Tank mass penalty for tank pressurization approach.

cluded. The resulting tank design pressure variation for the range of reactor power and run times considered is shown in figure 30.

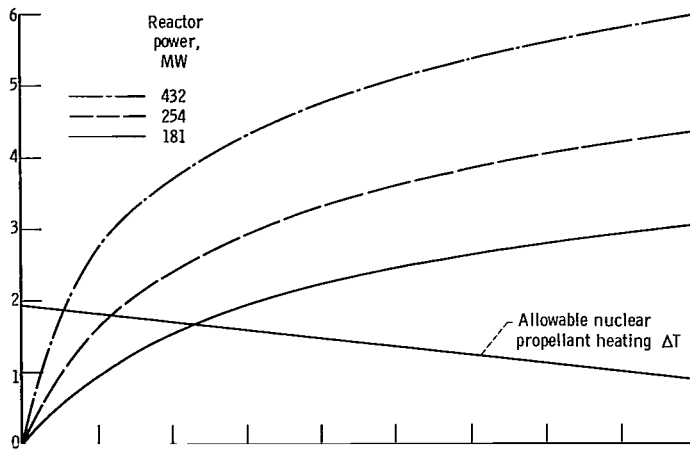
The effect of increased tank pressure on tank weight was based on a value of 1.84×10^{-3} kilogram of tank (including insulation) weight per newton per square centimeter of tank pressure increase per kilogram of propellant. This value was obtained from unpublished tank weight data in a Douglas preliminary study of nuclear stages using modified S-IVB stage design. The tank weight penalty is shown in figure 31 for the range of power and run time. The increase in tank pressure also results in an increase in the weight of residual gas, which was found to be a negligible weight penalty.

Reactor Shielding Approach

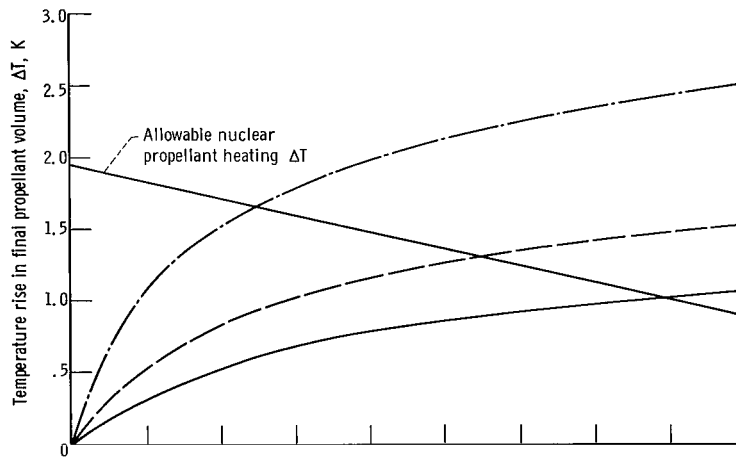
If boiloff is to be avoided in the shielding approach, the residual heating after a finite shielding attenuation must be absorbed by the nominal propellant subcooling. This subcooling is inherent in the typical propellant temperature (20.4 K) and tank design pressure (17.2 N/cm^2) conditions. The amount of shielding needed is therefore defined by the allowable nuclear bulk heating to just consume the allotted subcooling left after an allowance for the space environment heating, which is independent of shielding. This produces saturation temperature in the final propellant volume in the tank and corresponds to the zero NPSP condition for the final pump inlet flow in the shielded configuration. The shield weight thus defined is therefore the only weight penalty for this approach.

The assumed complete-propellant-mixing model required to utilize this nominal bulk subcooling relies, however, on complete turbulent mixing induced by the nuclear bulk heating. Hence, some remaining nuclear bulk heating must be allowed to support the complete-mixing model, and it is assumed that the allowable nuclear bulk heating defined herein is sufficient.

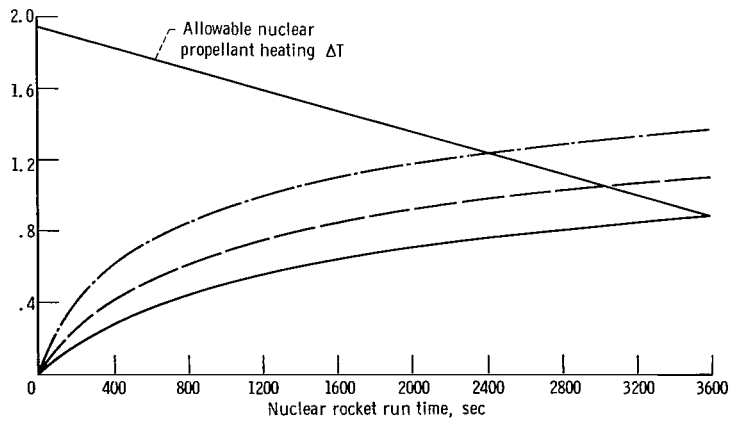
A 1.945 K propellant subcooling is available from the 20.4 K propellant supply temperature and 17.2-newton-per-square-centimeter typical tank design pressure. The space environment heating produces a final propellant temperature rise which varies with nuclear rocket run time and increases to a maximum of 1.05 K at 3600 seconds (see fig. 28). This assumes the high propellant heating rate of 295 watts per square meter as defined from consideration of tank insulation. When part of the propellant subcooling is used for the variable space environment heating, the remaining subcooling temperature rise for the shielded nuclear heating situation, shown in figure 28, represents the allowable nuclear propellant heating ΔT . At 3600 seconds run time, the allowable ΔT corresponds to full-tank heating rates of about 13, 16, and 23.5 kilowatts, for the 181-, 254-, and 432-megawatt reactor powers, respectively, which are assumed to support the



(a) Reactor-diameter shield.



(b) 120-centimeter-diameter shadow shield.



(c) Reactor-diameter shadow shield plus 20-gram-per-square-centimeter side shield.

Figure 32. - Nuclear bulk heating propellant temperature rise. Tank diameter, 6 meters; constant specific heat, 9.41×10^3 joules per kilogram per K; shield area density, 50 grams per square centimeter.

complete nuclear bulk mixing. The allowable ΔT is superimposed on the nuclear heating temperature rise data against reactor power and run time for a given shielded configuration, as for example in the no-shielding case in figure 27. The intersections then define the allowable run times and corresponding useable propellant W_p which produce saturation temperature and zero NPSP at the end of the run.

To estimate shield weight requirements that satisfy these criteria over the limited range of reactor power and run time, several approximate shield configurations were defined as follows. First, since the propellant heating is primarily due to gamma-ray attenuation, as shown in figure 24 (p. 42), the shield material was represented by the neutron and gamma-ray attenuation characteristics of aluminum. Its characteristics are typical of the common structural materials that might be used for the small degree of gamma attenuation encountered in this situation.

Second, figure 27 shows that the maximum temperature rise of the final propellant volume is of the order of 7 K with no shielding, while the allowable ΔT is 1 or 2 K in figure 28 (p. 45). A single shield thickness represented by a mass thickness of 50 grams per square centimeter and a gamma-ray attenuation factor of about 6.5 was therefore selected to bring the shielded temperature rise down to approximately the allowable range.

Third, to produce the necessary fine adjustment in shielded temperature rise values over the range of reactor power and run time, the geometry of the shield configuration was also varied somewhat. Initial calculations were performed for a shadow shield (50 g/cm^2 mass thickness) of reactor diameter. Figure 32(a) shows a reduction in ΔT of the order of only 30 to 40 percent. Although the attenuation factor is 6.5 through the shield, direct propellant heating beyond the shadow cone of the shielding diameter produces an average attenuation factor of about 1.6. In figure 33, which summarizes the shield weight variations with geometry for allowable nuclear heating ΔT , this low shield weight geometry is represented by the solid data points.

Similarly, figures 32(b) and (c) show the temperature rise for a constant 120-centimeter-diameter shadow shield (approximately twice the reactor diameters for the three reactor powers considered) and a reactor-diameter shadow shield with a three-quarter length, cylindrical side shield of 20 grams per square centimeter. Their shielding weights are also represented in figure 33 and define variation of shield weight for almost the total range of power and run time. The choice of shadow plus side shield arrangement (half-solid symbols in fig. 33) substantially reduces the shield weight compared with a full shadow shield (220 cm diam) weighing 2180 kilograms, which would be required for equivalent propellant heating reduction.

The asymptotic shape of the shield weight variation is coincidental because of the particular shield geometrical variations chosen to arrive at an estimate. Some reduction in shield mass at the intermediate values might be possible by alternate geometrical

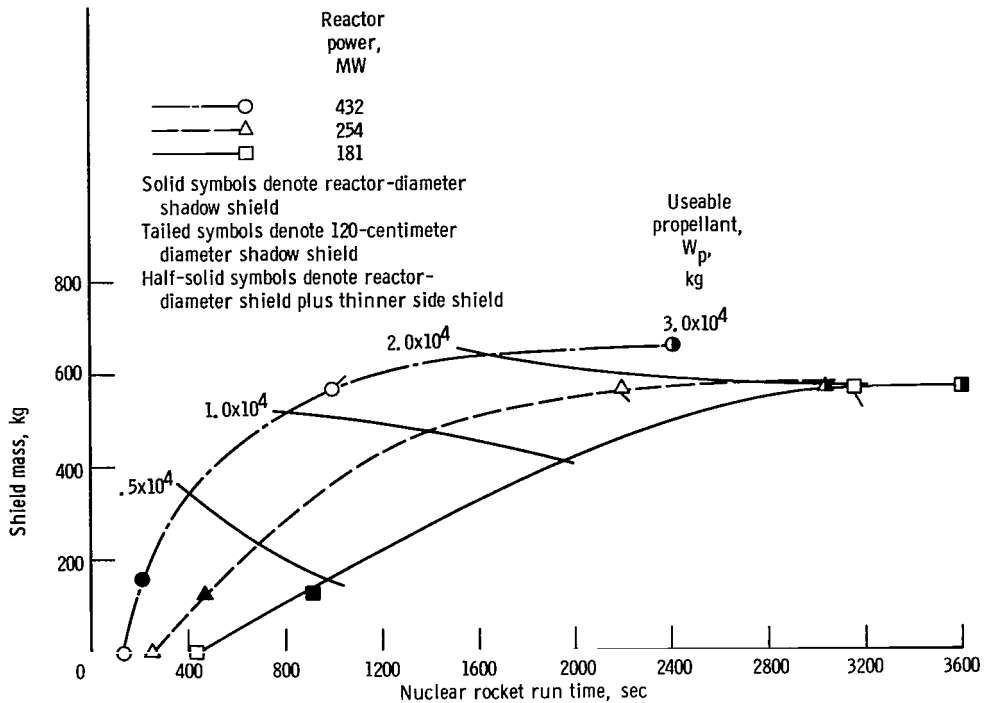


Figure 33. - Shield mass penalty for reactor shielding approach. All shadow shields of 50-gram-per-square-centimeter area density; zero NPSP at end of run time.

variations, but the estimate is considered adequate for the present study purposes. The subsequent payload performance analysis also showed no need for an estimate beyond about 30 000 kilograms of useable propellant. But such an extension of the 432-megawatt-reactor values to the assumed 3600-second-run-time limit of the graphite-fuel-element type would show a shield weight increase to approximately 820-kilograms, thereby illustrating the nonasymptotic behavior beyond the present range.

As in the propellant subcooling approach, any propellant stratification in the real situation could result in some boiloff for these estimated shield weights. Such an effect would require further shielding or a trade-off of boiloff for shield weight and in either case requires further detailed study of the thermodynamic and flow processes.

An added benefit of the shielding approach is the further reduction of the fast-neutron and gamma-ray dose to the payload. With no shielding, these doses are already below the previously set criteria, but the shielding weights could reduce the gamma dose, especially, by as much as a factor of 1/7 at the longer run times.

REFERENCES

1. Anon.: Preliminary Study of the NERVA II Reactor Design. Rep. WANL-TME-978, Westinghouse Astronuclear Lab., Sept. 30, 1964.
2. Anon.: Nuclear Rocket Technology Conference. NASA SP-123, 1966.
3. Clark, M. Ray: Reactor Physics Considerations and Weight Characteristics of Small Water-Graphite Nuclear Rocket Reactors. NASA TM X-1520, 1968.
- ✓ 4. Anon.: Parametric Nuclear Rocket Engine Data. Vol. 5 of Mission Oriented Advanced Nuclear System Parameters Study. Rep. STL-8423-6009-RL000, TRW Space Technology Lab., Mar. 1965.
5. Anon.: RIFT Safety Review Program - NERVA Systems Description. Rep. AGC-2421, Aerojet-General Corp., Nov. 1962.
- ✓ 6. Plebuch, R. K.; McDougall, J. R.; Spencer, R. B.; and Wener, K. R.: Detailed Technical Report, Nuclear Rocket Engine Analysis. Vol. 4 of Mission Oriented Advanced Nuclear System Parameters Study. STL-8423-6008-RL-000, TRW Space Technology Labs. (NASA CR-69886), Mar. 1965.
- ✓ 7. Anon.: Detailed Technical Report, Mission and Vehicle Analysis. Vol. 2 of Mission Oriented Advanced Nuclear System Parameters Study. Rep. STL-8423-6006-RU000, TRW Space Technology Lab. (NASA CR-67146), 1965.
8. Anon.: Rift Systems Analysis. Vol. I: Vehicle Description and Summary. Rep. NSP-63-96, Vol. 1, LMSC-A663144, Lockheed Missiles and Space Co. (NASA CR-58710), June 1964.
9. Anon.: Centaur Payload User's Manual. Rep GD/C-BNZ65-060, General Dynamics/Convair (NASA CR-72109), Aug. 1966.
10. Anon.: Summary. Vol. 1 of Modular Nuclear Vehicle Study, Phase II. Rep. LMSC-A830244, Lockheed Missiles and Space Co. (NASA CR-93851), Feb. 29, 1968.
11. Anon.: Nuclear Propulsion Module Systems Analysis. Vol. 2 of Modular Nuclear Vehicle Study, Phase II. Rep. LMSC-A830245, Lockheed Missiles and Space Co. (NASA CR-94378), Mar. 1, 1967.
12. Lahti, Gerald P.: QADHD Point-Kernel Radiation Shielding Computer Code to Evaluate Propellant Heating and Dose to Crew During Engine Operation. NASA TM X-1397, 1967.

13. Hamman, Donald J.; Drennan, James E.; Veazie, Walter H.; Shober, Fred R.; and Leash, E. R.: Radiation-Effects State-of-the-Art 1965-1966. Rep. REIC-42, Battelle Memorial Inst., June 30, 1966.
14. Campbell, W. E.; Fitts, J. J.; and Beveridge, J. H.: NPSP Selection for a Nuclear Rocket. Paper No. 67-476, AIAA, July 1967.
15. Anderson, B. H.; Huntley, S. C.; and Connolley, D. J.: Propellant Heating Studies with Wall and Nuclear Heating. Paper No. 64-WA/AV-8, ASME, Nov. 1964.
16. Anderson, Bernhard H.; and Danilowicz, Ronald L.: Analytical and Experimental Study of Nuclear Heating of Liquid Hydrogen. NASA TN D-2934, 1965.
17. Tatom, J. W.; Brown, W. H.; Knight, L. H.; and Coxe, E. F.: Analysis of Thermal Stratification of Liquid Hydrogen in Rocket Propellant Tanks. Advances in Cryogenic Engineering. Vol. 9, K. D. Timmerhaus, ed., Plenum Press, 1964, pp. 265-272.
18. Cook, G. A.; and Dwyer, R. F.: Fluid Hydrogen Slush - A Review. Advances in Cryogenic Engineering. Vol. 11, K. D. Timmerhaus, ed., Plenum Press, 1966, pp. 202-206.
19. Mann, D. B.; Ludtke, P. R.; Sindt, C. F.; and Chelton, D. B.: Liquid-Solid Mixtures of Hydrogen Near the Triple Point. Advances in Cryogenic Engineering. Vol. 11, K. D. Timmerhaus, ed., Plenum Press, 1966, pp. 207-217.
20. Keller, C. W.: Effects of Using Subcooled Liquid and Slush Hydrogen Fuels on Space Vehicle Design and Performance. Paper No. 67-467, AIAA, July 17-21, 1967.
21. Stanley, N. E.; and Elrod, C. W.: Generation and Loading of Triple Point Hydrogen for High Performance Aircraft, Boosters and Spacecraft. Paper No. 67-468, AIAA, July 17-21, 1967.
22. Schulte, L. O.; and Wheeler, D. D.: Saturn IB Payload Planner's Guide. Rep. SM-47010, Douglas Aircraft Co., Inc., June 1965.
23. Dawson, R. P.: Saturn IB Improvement Study (Solid First Stage), Phase II. Rep. SM-51896, vols. 1 and 2, Douglas Aircraft Co. (NASA CR-77129 and CR-77131), Mar. 30, 1966.
24. Anon.: Boeing Model 946 Burner II Solid Rocket Upper Stage. Vol. II: Launch Vehicle Characteristics and Performance Handbook. Rep. D2-82601-2, Boeing Co., Aug. 1965.
25. Anon.: Preliminary Investigation of Reactor Emergency Cooling Requirements for NERVA. Rep. WANL-TME-1644, Westinghouse Astronuclear Lab., Aug. 1, 1967.

26. Anon.: NERVA Flight Malfunction Studies. Rep. RN-S-0431, Aerojet-General Corp., Nov. 1967.
27. McKereghan, C. D., et al: Modular Nuclear Vehicle Study, Phase III, Nuclear Propulsion Module-Flight Safety Studies. Rep. LMSC-K-05-67-3, Lockheed Missiles and Space Co. (NASA CR-93144), Feb. 29, 1968.
28. Anon.: Nuclear Propulsion Module - Flight Safety Studies. Vol. 5 of Modular Nuclear Vehicle Study, Phase II. Rep. LMSC-A830248, vol. 5, Lockheed Missiles and Space Co. (NASA CR-90366), July 31, 1967.
29. Bussard, Robert W.; and Delauer, R. D.: Nuclear Rocket Propulsion. McGraw-Hill Book Co., Inc., 1958.
30. Lathrop, K. D.: DTF-IV, A Fortran-IV Program for Solving the Multigroup Transport Equation with Anisotropic Scattering. Rep. LA-3373, Los Alamos Scientific Lab., Nov. 12, 1965.
31. Lewis Research Center Staff: Sealed-Foam, Constrictive-Wrapped, External Insulation System for Liquid-Hydrogen Tanks of Boost Vehicles. NASA TN D-2685, 1965.
32. Steele, A. J.: Nuclear Vehicle Technology. Paper No. 65-589, AIAA, June 14-18, 1965.

FIRST CLASS MAIL

U.S. AIR MAIL PERMIT NO. 1000 WASHINGTON, D.C. 20546
POSTAGE WILL BE PAID BY ADDRESSEE
FIRST CLASS MAIL PERMIT NO. 1000 WASHINGTON, D.C. 20546
POSTAGE WILL BE PAID BY ADDRESSEE

POSTMASTER: If Undeliverable (Section 158
Postal Manual) Do Not Return

"The aeronautical and space activities of the United States shall be conducted so as to contribute . . . to the expansion of human knowledge of phenomena in the atmosphere and space. The Administration shall provide for the widest practicable and appropriate dissemination of information concerning its activities and the results thereof."

— NATIONAL AERONAUTICS AND SPACE ACT OF 1958

NASA SCIENTIFIC AND TECHNICAL PUBLICATIONS

TECHNICAL REPORTS: Scientific and technical information considered important, complete, and a lasting contribution to existing knowledge.

TECHNICAL NOTES: Information less broad in scope but nevertheless of importance as a contribution to existing knowledge.

TECHNICAL MEMORANDUMS: Information receiving limited distribution because of preliminary data, security classification, or other reasons.

CONTRACTOR REPORTS: Scientific and technical information generated under a NASA contract or grant and considered an important contribution to existing knowledge.

TECHNICAL TRANSLATIONS: Information published in a foreign language considered to merit NASA distribution in English.

SPECIAL PUBLICATIONS: Information derived from or of value to NASA activities. Publications include conference proceedings, monographs, data compilations, handbooks, sourcebooks, and special bibliographies.

TECHNOLOGY UTILIZATION PUBLICATIONS: Information on technology used by NASA that may be of particular interest in commercial and other non-aerospace applications. Publications include Tech Briefs, Technology Utilization Reports and Notes, and Technology Surveys.

Details on the availability of these publications may be obtained from:

**SCIENTIFIC AND TECHNICAL INFORMATION DIVISION
NATIONAL AERONAUTICS AND SPACE ADMINISTRATION
Washington, D.C. 20546**